Project information

Project full title	European network for developing new horizons for RIs
Project acronym	EURIZON
Grant agreement no.	871072
Instrument	Research and Innovation Action (RIA)
Duration	01/02/2020 – 31/01/2024
Website	https://www.eurizon-project.eu/

Deliverable information

Deliverable no.	D3.2 (D17)
Deliverable title	Model calculations of VCN yields of converter/reflector for a VCN source
Deliverable responsible	ESS
Related Work-Package/Task	WP3, Task 3.3 Development of advanced Very Cold Neutron Source
Type (e.g. Report; other)	Report
Author(s)	Zsófia Kókai, Luca Zanini, José Ignacio Márquez Damián, Valentina Santoro
Dissemination level	Public
Document Version	1
Date	2022. 08. 31
Download page	

Document information

Version no.	Date	Author(s)	Comment
1	2022. 08 31.	Zsófia Kókai, Luca Zanini, José Ignacio Márquez Damián, Valentina Santoro	

This project has received funding from the European Union's Horizon 2020 research and innovation programme under grant agreement No. 871072.

1 Table of Contents

This project has received funding from the European Union's Horizon 2020 research and innovation programme under grant agreement No. 871072.

This project has received funding from the European Union's Horizon 2020 research and innovation programme under grant agreement No. 871072.

Model Calculations of VCN intensity of converter/reflector for a VCN source

2 Executive Summary

A comprehensive study of the intensity of Very Cold Neutrons (VCNs) from different moderator and converter materials was performed by Monte Carlo calculations using MCNP6.2 [1]. The goal of the study was to investigate the performance of such materials to generate VCNs, and to couple such materials with a reflector of nanodiamonds (NDs), in view of a possible prototype experiment for an advanced VCN source.

The choice of candidate VCN converter materials was based on expectations of good performance, and on the availability of thermal scattering cross sections in ACE format to be used in MCNP. The following materials were analysed: solid para- and orthodeuterium at 5 K, liquid para- and orthohydrogen at 14 K and solid methane at 22 K.

The calculations were carried out using the MCNP 6.2 code. A cylindrical converter was irradiated by a collimated cold neutron beam from the side. A sensitivity study was performed varying the height and diameter of the moderator: the height of the moderator was changed between 1 and 50 cm, the diameter was changed between 2 and 100 cm.

The cold neutron (CN) source was defined by the description of the beam characteristics of the first ballistic supermirror neutron guide H113 that feeds the neutron user facility for particle physics PF1B of the Institute Laue-Langevin, Grenoble (ILL), where a prototype experiment is intended to be performed.

It can be concluded that the maximum intensity is given by the biggest size solid deuterium converter (100 cm diameter, 50 cm height). In terms of realistic sizes for an experiment demonstration (3 cm diameter, 1 cm height) liquid orthohydrogen and solid methane gave the maximum output.

The second part of the analysis consisted in introducing a nanodiamond (ND) reflector in the extraction system of the converter. For this configuration, we used the small-geometry of the converter (3 cm diameter, 1 cm height), and the surrounding nanodiamond reflector was 16 cm high.

The gain in the performance of the VCN source was computed at the exit of the ND reflector, in which case neutrons at all divergences are computed, and also at 1 m distance from the system, to calculate the gain for low-divergence neutrons, which is of greater interest for applications for neutron scattering instruments.

This project has received funding from the European Union's Horizon 2020 research and innovation programme under grant agreement No. 871072.

At the exit of the ND reflector an increase by about a factor of 40 was predicted when using the deuterium converter, an increase by a factor of 13-14 was observed when hydrogen converter was used, while an increase by a factor of 16 was calculated when the converter material was methane. These gains were computed considering neutrons with wavelength greater than 40 Å.

The angular distribution shows that most of the increase is due to high-divergence neutrons. Therefore, this increase can be measured only at the exit of the ND reflector.

For low-divergence neutrons, at 1 m from the source an increase by a factor of 3 was computed when using the paradeuterium converter, an increase by a factor of 4 was observed when orthodeuterium converter was used, an increase by a factor of 3.5 was predicted when the converter material was parahydrogen, while an increase by a factor of 2 was calculated when using orthohydrogen or methane converters. At 1 m from the source, flux was calculated by 5 cm diameter spherical volume detector tally (the solid angle is 3°). This result is quite interesting because these are low divergence neutrons, usable in neutron scattering experiments. We would expect to observe such a gain in the prototype experiment.

As a comparison with NDs, we considered a similar geometry where supermirrors with m=6 replace the NDs. With a methane converter, an increase by a factor of 9 was computed at 16 cm from the source, but only 10 % gain was observed at 1 m from the source.

This project has received funding from the European Union's Horizon 2020 research and innovation programme under grant agreement No. 871072.

3 Introduction

Within the EURIZON (European network for developing new horizons for RIs) project [2] in the Work Package 3 the Task 3.3 is dedicated to develop an advanced Very Cold Neutron (VCN) source.

Cold neutron sources have been used for decades in many research facilities, mostly research reactors and spallation sources. They are fairly easy to build and generally utilize neutron moderators using liquid hydrogen or deuterium. The spectral distribution of neutrons from such moderators peaks between 2 and 3 Å, and decreases with the neutron wavelength increase, in agreement with a Maxwell-Boltzmann distribution. The moderators are at temperatures around 20 K.

There is however interest in sources delivering higher neutron fluxes at longer wavelengths than what provided by cold sources. We consider Very Cold Neutrons (VCNs), neutrons having energy between the cold neutron and ultracold neutron energy range, approximately between 10 and 100 Å.

At present, there is only one VCN beamline in the world: the PF2 neutron beamline at ILL [3]. The VCN neutrons are extracted vertically from one of the two cold sources in the reactor core, containing liquid deuterium [3].

The definition of the wavelength range of VCNs is not unambiguous.

According to Ref. [3], VCNs are in the range of energies that approximately correspond to thermal equilibrium at the lowest practical moderator temperature, that of superfluid helium, Tc≤2.17 K at 1 atm. The corresponding energy is $E_{vcn}=k_bT=187\mu eV$, VCNs follow the "rule of 2s" [4]:

$$T \approx 2K, \qquad E \approx 200\ \mu eV, \qquad v \approx 200\frac{m}{s}.\lambda \approx 20\ \text{Å}$$

In the same reference, the VCN range is defined between 10 Å and 100 Å. Another classification of VCN range depends on their intended use, which can be for fundamental physics experiments, or for neutron scattering. In the former case, the range of interest starts at about 40 Å and extends to the UCN wavelengths, i.e. about 600 Å. In the latter case, VCNs are rather an extension of the cold range, i.e., between 10 Å and 40 Å, which is a bandwidth usable for some neutron scattering applications such as spin echo and SANS, where a measuring also at longer wavelengths than conventionally done could give significant advantages [5].

In this work we looked at neutrons up to 90 Å. This is dictated by a limitation of MCNP, which transports neutrons down to 0.1 µeV.

The main objectives of this deliverable are:

This project has received funding from the European Union's Horizon 2020 research and innovation programme under grant agreement No. 871072.

1. Study and compare the performance of candidate converter materials to produce a flux of VCN starting from a beam of cold neutrons.
2. Study of the VCN reflector to be coupled to the converter for an efficient transport of VCNs

This project has received funding from the European Union's Horizon 2020 research and innovation programme under grant agreement No. 871072.

4 Applications of VCN

Very cold neutrons can be used effectively for various applications in fundamental physics [6]. Some example of applications include:

- Various experiments could be used for phenomenological constraint for extra short range forces [7].
- Precision measurement of the neutron whispering gallery quantum states [8]. The advantage compared to using cold neutrons consists in the possibility of selective populating low deeply-bound quantum states with low tangential momentum. Such quantum states would be particularly sensitive to extra short-range interactions. The advantage compared to using UCN consists in significantly larger statistics.
- Precision studies of the neutron β-decay (in-flight measurements of the neutron lifetime and the asymmetry coefficients in the neutron β-decay). Using slower neutrons increases the probability of the β-decay [9].
- Measurements of nuclear reactions induced by polarized slow neutrons [10].

In addition to that, there are indications that VCNs can be applied to neutron scattering, for various applications [5].

This project has received funding from the European Union's Horizon 2020 research and innovation programme under grant agreement No. 871072.

5 Concept for a VCN

The concept for a VCN source investigated in this work consists of two main components: 1) a suitable converter material that will deliver a high intensity of VCNs, and 2) an advanced reflector to efficiently transport these VCNs to the experiment. We discuss separately these two components.

5.1 Converter material

Concerning the first component, it is important to make a distinction between moderator and converter. In a moderator, thermal equilibrium is reached between the neutrons in the moderator and the moderator medium, and the neutron spectrum has a Maxwell-Boltzmann distribution. One typical example is the neutron spectrum from a water moderator. Usually there are some deviations from the Maxwellian distribution, due to effects such as the finite size of the moderator, or a non-negligible neutron absorption cross section, but the distribution is usually very close.

The situation is different in a so-called converter. In this case the neutron spectrum is at a higher temperature with the medium. The neutron kinetic energy is lost with a different mechanism than neutron moderation, i.e. in a single inelastic transition which strongly lowers the kinetic energy. The low temperature of the medium reduces neutron upscattering and thus increases the intensity of CNs or VCNs. One example is the phonon transition in liquid helium, which converts neutrons of 8.9 Å directly to the UCN regime. In this sense, parahydrogen can be considered a converter, in particular in a compact geometry of low-dimensional moderators [11]: in fact, in parahydrogen there is typically a single transition from thermal to cold energy, due to the spin-flip of one of the protons in the hydrogen molecule, resulting in an energy loss of the neutron of about 14 meV.

The first task in the design of a VCN source is to determine the best material for the moderator/converter. This includes also determining its dimensions. It is foreseen that a few selected materials will be chosen as candidates for further studies.

The type of converter depends also on the spectrum of incoming neutrons, which typically can be either a thermal spectrum (e.g. in a reactor source or a thermal beamline) or a cold spectrum coming from a cold moderator. In this work we concentrate on the second option, because the goal is to make a prototype experiment (see Section 6) at the ILL cold beamline [12].

5.2 Reflector material

Once the material is selected, the second stage of the source design consists in coupling the material with suitable reflectors with the aim to increase the flux of VCNs in the direction where the beamline is placed.

This project has received funding from the European Union's Horizon 2020 research and innovation programme under grant agreement No. 871072.

A good reflector material should have the property of reflecting VCNs and having a low absorption cross section. The first candidate material that is considered is formed by diamond nanoparticles. This material has been studied extensively from the theoretical and experimental sides, in the last 15 years. It has very interesting properties of high albedo for neutrons in the VCN range, and of quasi-specular reflection for cold neutrons [13] [14] [15] [16] [17].

The reflector must be coupled to the moderator/converter in order to maximize the performance of the VCN source. For this optimization, a figure of merit is defined (see chapter 12).

This project has received funding from the European Union's Horizon 2020 research and innovation programme under grant agreement No. 871072.

6 Concept for a VCN prototype experiment

In this paragraph we show a schematic model of a possible prototype experiment that was discussed at the beginning of the project. The schematic of the experiment is shown in Figure 1 [2].

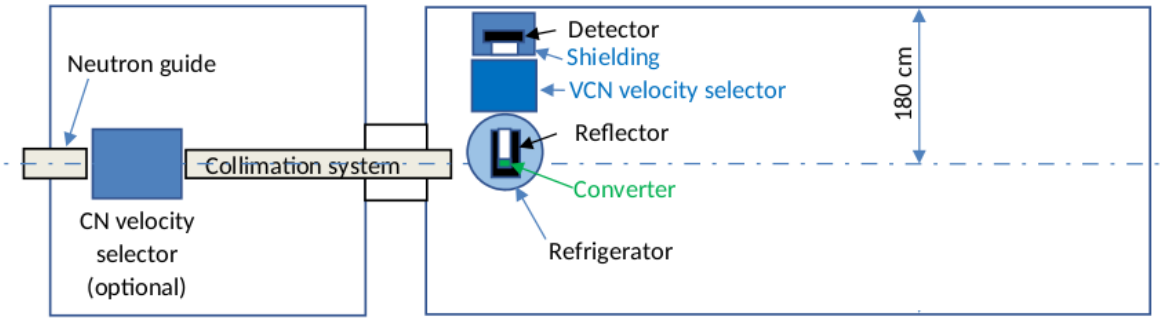

Figure 1. Concept for the experiment by E. Lychagin, V. Nesvizhevsky et al. See explanation in the text

A collimated cold neutron beam impinges a 3 cm diameter cylindrical converter surrounded by a 3 cm thick ND reflector (VCN source). The converter is at cryogenic temperatures (e.g. 5 K if solid deuterium is used), while it needs to be defined if the reflector will be at room or cryogenic temperature. The moderated and scattered neutrons are detected at the top of the converter. A velocity selector is placed after the VCN source to allow spectral measurements. The distance between the detector and the VCN source is about 2 m.

This project has received funding from the European Union's Horizon 2020 research and innovation programme under grant agreement No. 871072.

6.1 Source term

The incoming cold neutron spectrum to be used in the simulations was defined based on the spectrum of the ILL vertical cold neutron source which consists of about 20 litres of liquid deuterium at 25 K (see Figure 2).

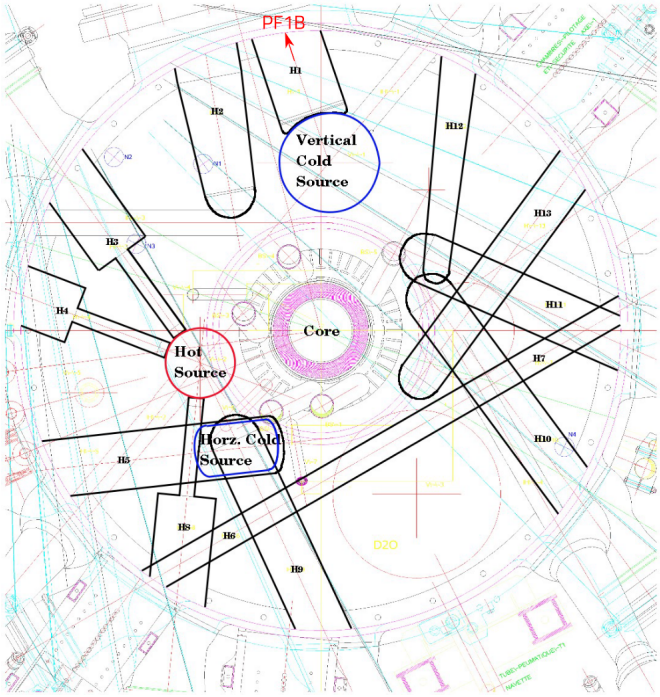

Figure 2 Geometry of the ILL source showing the reactor core, the heavy water vessel, the cold and hot sources, and beam inserts. The prototype experiment is intended to be performed at the PF1B beamline which is pointing at the "Vertical Cold Source" [18]

We used the description of the beam characteristics of the first ballistic supermirror neutron guide H113 that feeds the neutron user facility for particle physics PF1B of the Institute Laue-Langevin in Grenoble (ILL)] [12]. An analytic approximation to the measured on-axis brightness $B_C(\lambda)$ was given. Empirically cold neutron wavelength spectra often are better described by an exponential $\exp(-\lambda/\lambda_1)$, multiplied by a short-wavelength cut-off function, rather than by a Maxwellian spectrum [12].:

$$B_c(\lambda) = B_0 \cdot \frac{(\frac{\lambda}{\lambda_2})^p}{1+(\frac{\lambda}{\lambda_2})^p} \cdot e^{-\frac{\lambda}{\lambda_1}} \qquad \text{(Eq. 1)}$$

λ_1=0.33 nm, λ_2=0.4 nm, p=3, B_0= 1.3x10^{11} cm^{-2} s^{-1}nm^{-1}

This project has received funding from the European Union's Horizon 2020 research and innovation programme under grant agreement No. 871072.

The particle flux is 2.7 times lower than the capture flux density.

The PF1B spectrum is shown in Figure 3. On the figure both the measured spectrum and the fitted spectrum using Eq. 1 are shown.

For the source intensity we multiplied the particle flux by the source area (1 cm diameter circle).

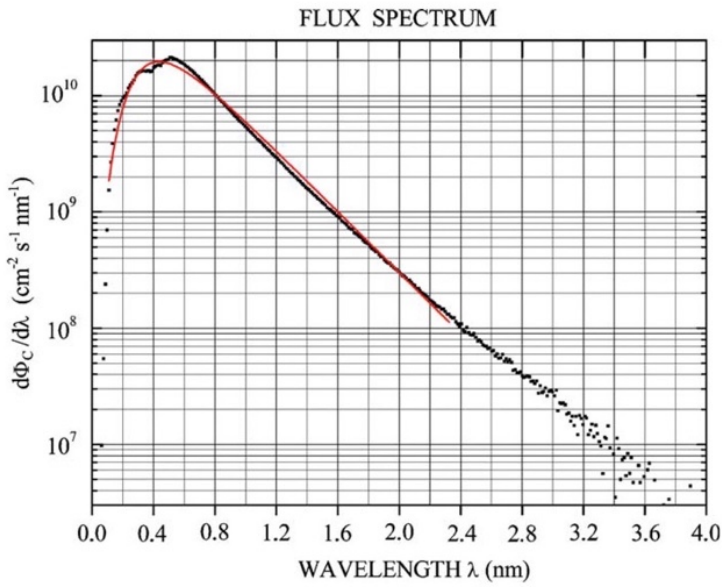

Figure 3 Neutron spectrum of PF1B neutron beam at ILL: measured and fitted spectrum from Ref. [12]

This project has received funding from the European Union's Horizon 2020 research and innovation programme under grant agreement No. 871072.

7 Candidate materials for moderator/converter

In this section we discuss the candidate materials for a VCN source

The list of candidate materials is shown in Table 1.

Table 1 Candidate moderator/converter materials

Material	Temperature	Density (g/cm^3)
Solid paradeuterium	5 K	0.2059
Solid orthodeuterium	5 K	0.2059
Liquid parahydrogen	14 K	0.071
Liquid orthohydrogen	14 K	0.071
Solid methane	22 K	0.5

For the converter solid deuterium and liquid hydrogen at 14 K were selected, both in para and ortho state, as well as solid methane at 22 K.

A molecule of dihydrogen contains two atoms, and the nuclei of both atoms have angular momentum. Depending upon the direction of the spin of the nuclei, the hydrogens are of two types: Orthohydrogen molecules are those in which the spins of both the nuclei are in the same direction. Molecules of hydrogen in which the spins of both nuclei are in the opposite direction are called parahydrogen [19]. Similar to the hydrogen molecule, deuterium molecules have separable nuclear spin isomers denoted as “ortho” and “para.” In short, spin isomers exist in the deuterium molecule due to the parity between the nuclear spin function and rotational spin function. For simple, isotopic diatomic molecules, the rotational spin, J, of the two nuclei can either be symmetric (J = 0, 2, 4, …) or antisymmetric (J = 1, 3, 5, …). As deuterium cools to cryogenic temperatures, insufficient energy is available to populate higher-energy modes. Approaching absolute zero, molecules in the even J states de-excite to J = 0, while molecules in the odd J states de-excite to J = 1. Deuterium molecules below 50 K in the J = 1 rotational state are metastable and may take days or weeks to de-excite to the J = 0 rotational state in the absence of a suitable catalyst. This parity allows for two separable and interconvertible deuterium forms. Contrary to hydrogen and tritium, the lower-energy, even-J states are denoted “ortho” for deuterium, while the higher energy, odd-J states are denoted “para.” [20]

This project has received funding from the European Union’s Horizon 2020 research and innovation programme under grant agreement No. 871072.

The criteria for the selection of the materials were based on expected good performance for VCN production (see e.g. [21]), and availability of thermal scattering cross sections.

It should be mentioned that clathrate hydrates are very promising candidates for VCN moderators, however they have not been tested in this work because the thermal scattering libraries are still under development within the HighNESS project [22] . Molecular oxygen with its triplet ground state appears particularly promising, notably as a guest in fully deuterated O_2-clathrate hydrates. Other possibilities are dry O_2–^{4}He van der Waals clusters and O_2 intercalated in fcc-C_{60} [23].

This project has received funding from the European Union's Horizon 2020 research and innovation programme under grant agreement No. 871072.

8 Candidate materials for reflectors

For reflector materials, we considered pure nanodiamond (NDs), see Table 2. with its properties. A comparison with expected performance from supermirrors was also done.

Table 2 Candidate reflector materials

Material	Temperature	Density (g/cm^3)
Nanodiamond	296 K	0.6 (bulk density)

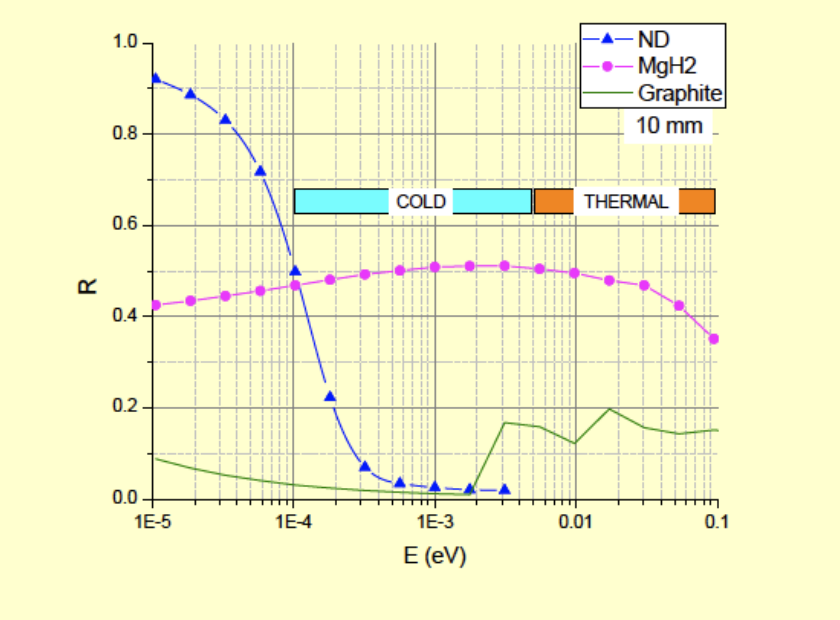

Figure 4 Albedo of nanodiamond, magnesium-hydride and graphite [11]

In Figure 4 the reflection of NDs are compared with magnesium hydride [24], which is a good reflector for cold neutrons, but for the very cold range the NDs have better properties, therefore we did not consider it for our setup. Other possibilities include conventional reflectors such as beryllium at room temperature.

This project has received funding from the European Union's Horizon 2020 research and innovation programme under grant agreement No. 871072.

9 Definition of neutron mirror

The reflectivity R of a neutron guide in MCNP is described analogously to the definition used in McStas [25]:

$$R = R_0; Q \leq Q_c$$
$$R = \frac{R_0}{2}\left\{1 - tanh\left(\frac{Q - mQ_c}{W}\right)\right\}\{1 - \alpha(Q - Q_c)\};\ Q \geq Q_c \qquad \text{(Eq.2)}$$

with the constant reflectivity R_0 for values of the scattering vector Q smaller than the critical momentum transfer Q_c. Q_c is the largest scattering vector that a single layer of mirror material would allow. The parameter α describes the declining of the reflectivity between values Q and mQ_c with m carrying values larger than or equal to unity. This decline is typical for so-called supermirror surfaces that extend the total reflectivity properties of neutron mirrors to scattering vectors of mQ_c. The parameter *W* defines the level of smearing at the edge of the reflectivity around mQ_c.

In MCNP the user is able to specify the parameters of the guide using a so-called REFF card [26]. Here, *Ro* is set to 0.99, *Qc* to 2.19 X 10^{-2} Å^{-1}, *m* to 6, α to 6.07 Å, and *W* to 3 X 10^{-3} Å^{-1} similarly as it was given in Ref [26].

This project has received funding from the European Union's Horizon 2020 research and innovation programme under grant agreement No. 871072.

10 Thermal scattering cross sections

In this section, we describe the thermal scattering cross sections for the materials used in this work, starting with a classification of the interactions that are treated.

In the energy range where thermal scattering cross sections need to be considered, i.e., below about 100 meV there are three different possible interactions: inelastic, elastic (Bragg or incoherent) and small angle neutron scattering (SANS), which is also an elastic scattering.

In inelastic neutron scattering there is an exchange of energy between the material and the neutrons. This is dependent on the atom bonding and the resulting phonon spectra.

The Bragg scattering is due to interference from the different planes of atoms in the crystal. It has a cutoff energy, because longer wavelength neutrons than some value cannot satisfy the Bragg condition given by

$$2d \sin\theta = n \lambda \qquad \text{(Eq.3)}$$

where d is the lattice spacing, θ is the scattering angle, n is a sequential number n=1,2,,…, and λ is the wavelength.

The SANS scattering is coming from the interference of the neutron wave with bigger particles, of the size of tens of ångstroms.

Liquid materials only present inelastic scattering. Solid materials present inelastic scattering and elastic scattering. SANS is only present if the material has structures in the nanometric scale, either particles or pores.

This project has received funding from the European Union's Horizon 2020 research and innovation programme under grant agreement No. 871072.

10.1 Solid methane

Solid methane in phase I at 22 K was modelled using the evaluation distributed with ENDF/B-VIII.0. which was based on the Harker-Brugger spectrum [27]. Compared with the libraries distributed with MCNP, the elastic cross section was rescaled to give the correct asymptotic value at low energies [24]. The scattering cross section of solid methane is shown in Figure 5.

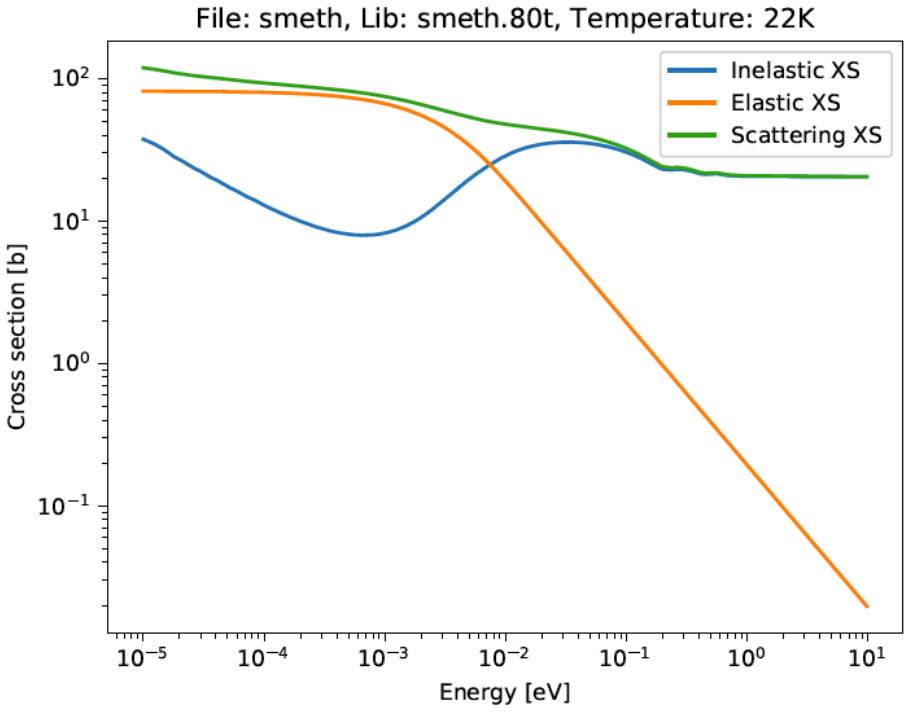

Figure 5 Scattering cross sections of solid methane at 22 K ENDF/B-VIII.0 evaluation processed with NJOY21 version 1.1.1. [28] The elastic component was renormalized.

This project has received funding from the European Union's Horizon 2020 research and innovation programme under grant agreement No. 871072.

10.2 Nanodiamonds

Diamond nanoparticles (NDs) are in nanosized powder form, and can be produced by detonation and other methods. Their particle size is typically in the order of 5 nm, which generates significant small angle neutron scattering effect for neutrons with wavelengths in the 10-100 Å range. Since SANS is elastic, NDs could be used to improve the reflective properties of a system.

In practice, SANS starts to produce a significant reflection effect below 0.1 meV (Fig. 6), which makes NDs most useful as a VCN / UCN reflector.

Thermal scattering in NDs was represented as a combination of a model for pure bulk diamond in NJOY, providing coherent elastic and inelastic cross section, and a hard coded SANS model implemented in MCNP based on experimental data from Teshigawara [29]. The composition of the material used in MCNP only includes carbon, thus resulting in a model for ideal nanodiamond powder without impurity effects in absorption or inelastic scattering. Further improvements from fluorination were not considered [13].

The resulting thermal scattering cross section is shown in Figure 6.

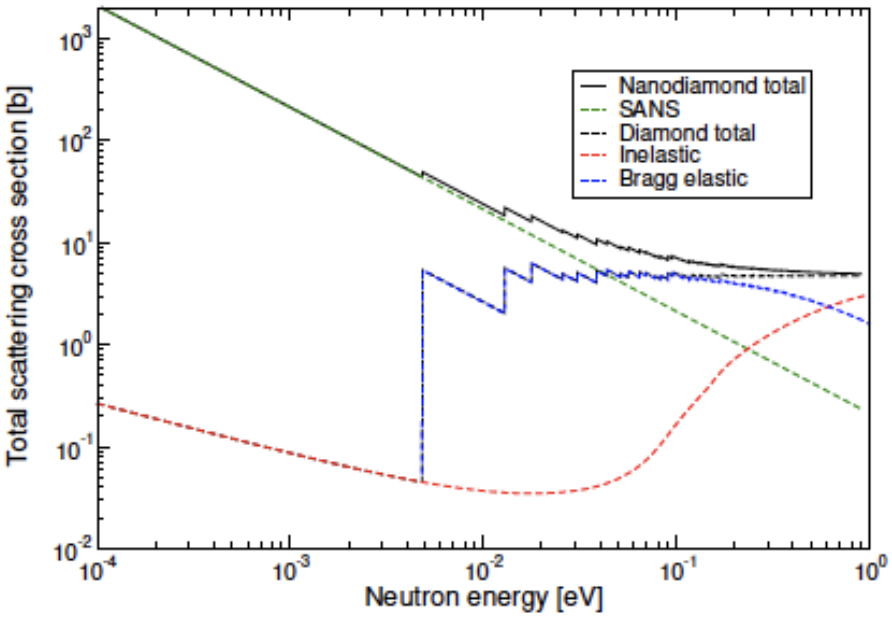

Figure 6. Neutron cross sections for NDs

This project has received funding from the European Union's Horizon 2020 research and innovation programme under grant agreement No. 871072.

10.3 Solid deuterium

The thermal scattering library for solid deuterium was developed using NJOY+NCrystal [30]. based on a model by Granada [31]. The resulting ACE file was prepared in the mixed-elastic format, which requires a custom version of MCNP6 or PHITS to run.

Figure 7 and 8 show the different components of the scattering cross section for solid ortho- and paradeuterium, respectively, at 5K. Contrary to other materials that have either an incoherent or coherent component to the scattering cross section, solid deuterium has a significant contribution from both coherent and incoherent elastic scattering, which requires using the mixed elastic format [30].

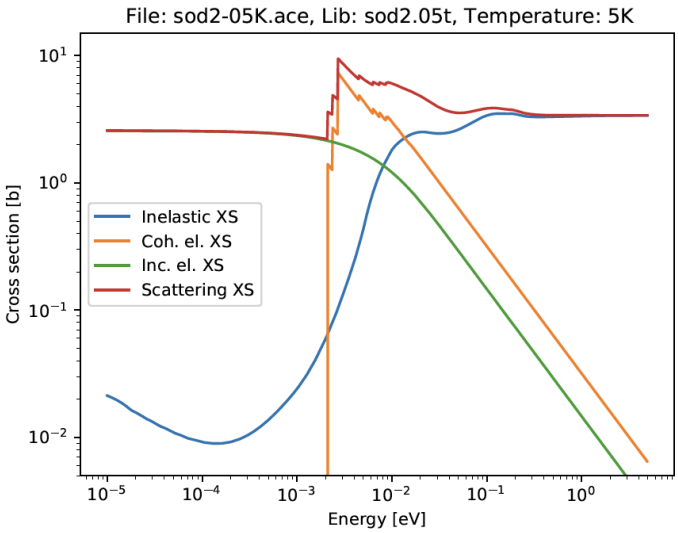

Figure 7. Scattering cross sections of solid orthodeuterium at 5K

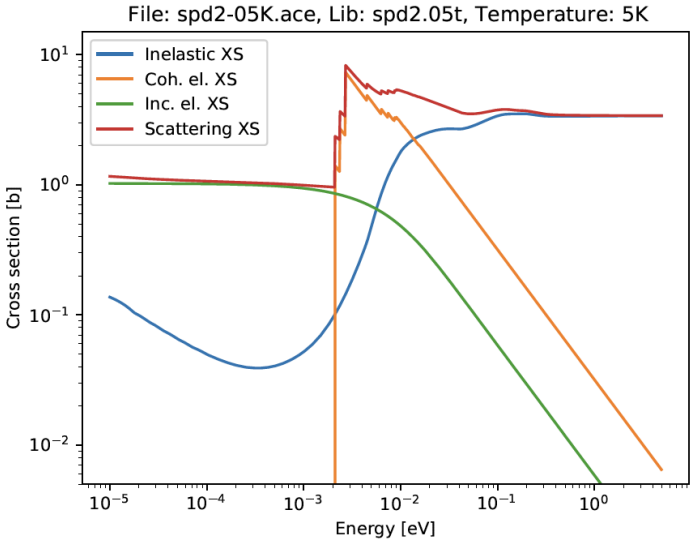

Figure 8 Scattering cross sections of solid paradeuterium at 5K

This project has received funding from the European Union's Horizon 2020 research and innovation programme under grant agreement No. 871072.

10.4 Liquid hydrogen and deuterium

Libraries for liquid hydrogen at 14K were obtained from JEFF 3.3 library [32] which includes an improved version of the model developed at evaluation from Centro Atomico Bariloche [33]. The libraries were processed on a fine angular and energy grid [34] with NJOY21 version 1.1.1.

Figure 9 and 10 show plots of the scattering cross section for liquid para- and orthohydrogen respectively, at 14K.

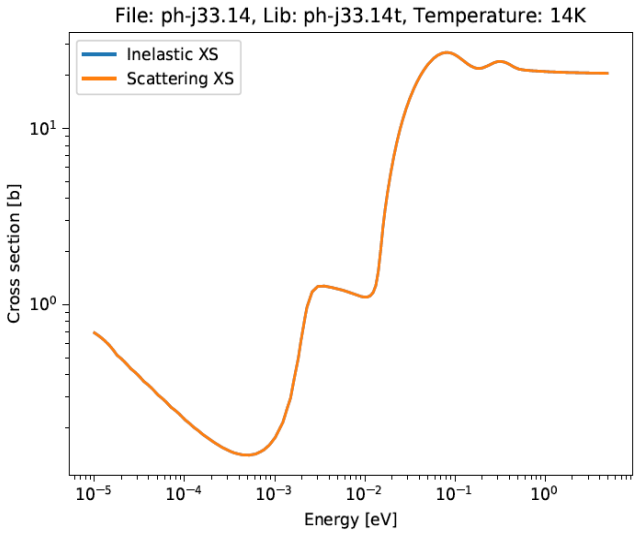

Figure 9 Scattering cross sections of liquid parahydrogen at 14 K (it has only inelastic part)

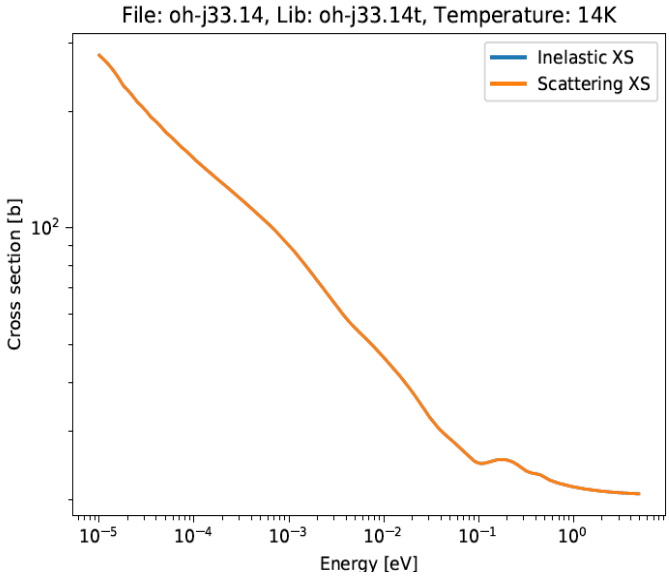

Figure 10 Scattering cross sections of liquid orthohydrogen at 14 K (it has only inelastic part)

This project has received funding from the European Union's Horizon 2020 research and innovation programme under grant agreement No. 871072.

10.5 Neutron mean free path in different materials

Figures 11 and 12 show the neutron mean free path in different converters. The mean free path of VCN is the mm range in solid methane and liquid orthohydrogen, they work in cm scale as VCN converters. In liquid parahydrogen and solid deuterium (both ortho and para), the mean free path of VCN is in dm scale, which implies larger size for VCN converters.

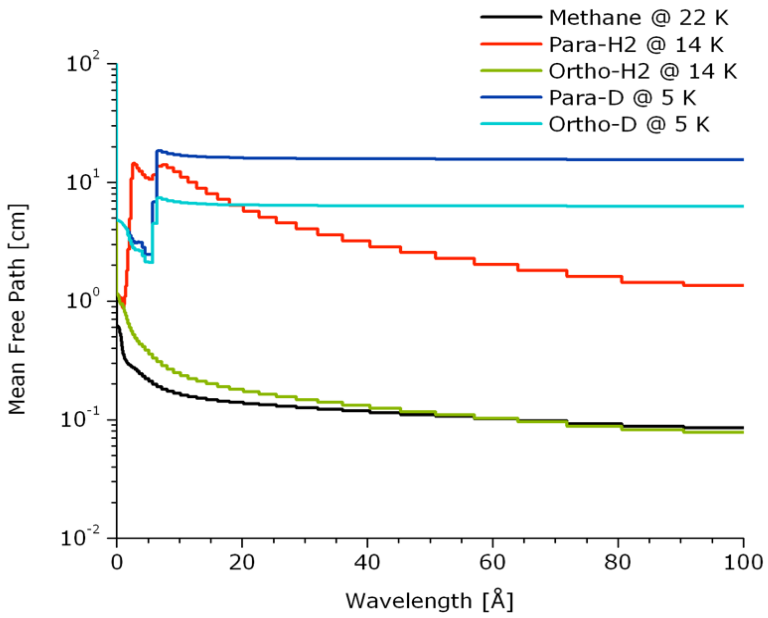

Figure 11. Neutron mean free path as a function of neutron wavelength for different moderators

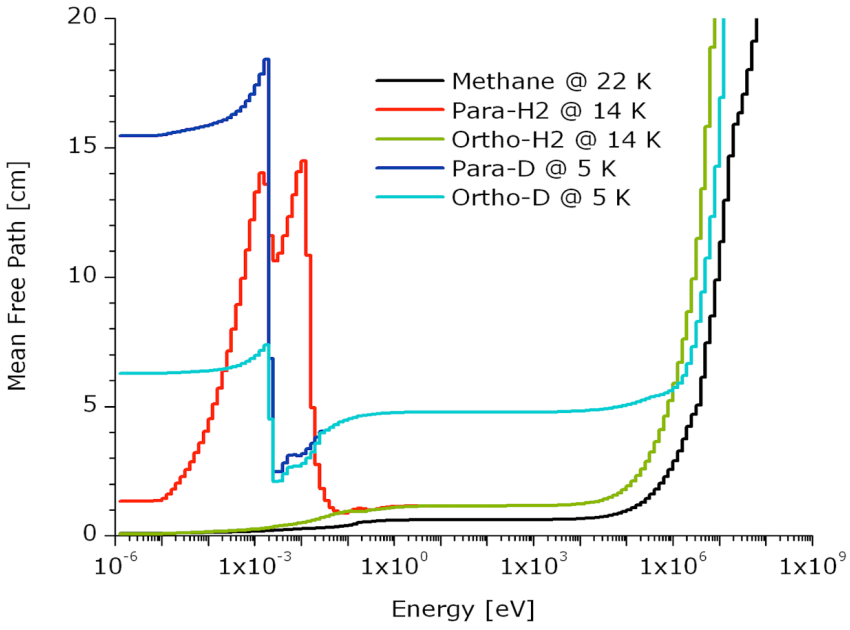

Figure 12. Neutron mean free path as a function of energy for different moderators

This project has received funding from the European Union's Horizon 2020 research and innovation programme under grant agreement No. 871072.

11 Monte Carlo methodology

The calculations were carried out by using the MCNP6 code, version 6.2. [35]. The MCNP6 code, developed and maintained by Los Alamos National Laboratory, is an internationally recognized code for calculating the transport of particles by the Monte Carlo method. MCNP6 treats geometry problems primarily in terms of regions or volumes bounded by first and second-degree surfaces. Cells are defined by intersections, unions, and complements of the region, and contain user defined materials. The characteristics of the source (particle type, energy distribution, geometry) are also defined by the user MCNP6 uses estimator methods to calculate particle fluxes and reaction rates. The formalism of estimators is called tallies.

The ENDF/B-VIII.0 data library was used except for the thermal scattering libraries as referenced in Section 10.

11.1 Geometry for neutron intensity of bare converter

To calculate the neutron intensity from a bare converter, we modelled a cylindrical converter. The source term consisted of a neutron beam with the energy spectrum defined from Section 6.1. The beam footprint was circular with 1 cm diameter, hitting the cylinder from the side (Figure 13). A sensitivity study was performed varying the height and diameter of the moderator: the height of the moderator was changed between 1 and 50 cm, while the diameter was changed between 2 and 100 cm. The converter is placed in a 1 mm thick aluminium holder. In the case of deuterium, a 30 µm thick aluminium holder and 1 mm beryllium holder were also studied.

The outcoming neutron flux was calculated at 1 m distance from the converter using point detector (F5) tallies and 5 cm diameter sphere volume detector(F4) tallies at 1 m (Figure 13). The angular distribution of the outcoming neutrons is measured at 16 cm and 1 m distance from the source beam by surface detector (F1) tally.

This project has received funding from the European Union's Horizon 2020 research and innovation programme under grant agreement No. 871072.

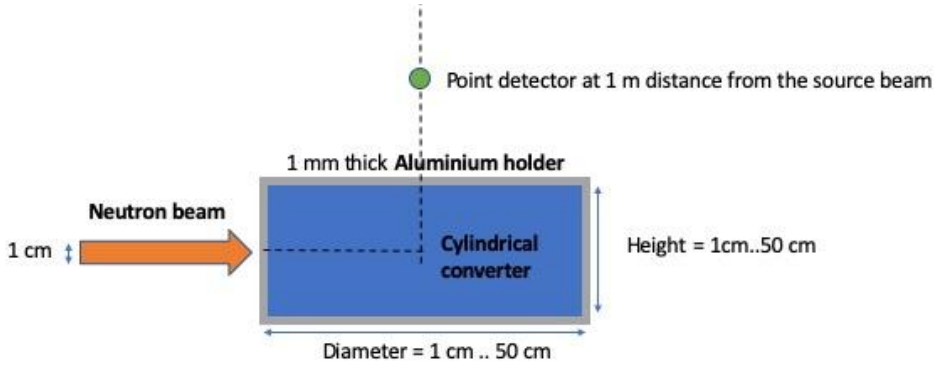

Figure 13. Geometry for the calculation of the intensity of a bare converter, showing position of the tallies, the height of the moderator is varied between 1 and 50 cm, the diameter is varied between 2 and 100 cm.

This project has received funding from the European Union's Horizon 2020 research and innovation programme under grant agreement No. 871072.

11.2 Geometry of converter/reflector

This geometry is a simplification of the experiment intended to be performed at PF1B.

A 3 cm diameter, 1 cm height cylindrical converter placed into a 1 mm thick aluminium holder in case of hydrogen and methane, and 30 µm thick aluminium holder in case of deuterium. It is surrounded by a 3 cm thick nanodiamond reflector. The nanodiamond is not placed in an additional holder. The converter is impinged by neutrons from the side. The neutron source is a 1 cm diameter cylindrical cold neutron source (Figure 14). The outcoming neutron flux is measured at 1 m distance from the source beam by volume detector (F4) tally. The angular distribution of the outcoming neutrons is measured at 16 cm and 1 m distance from the source beam by surface detector (F1) tally (Figure 15).

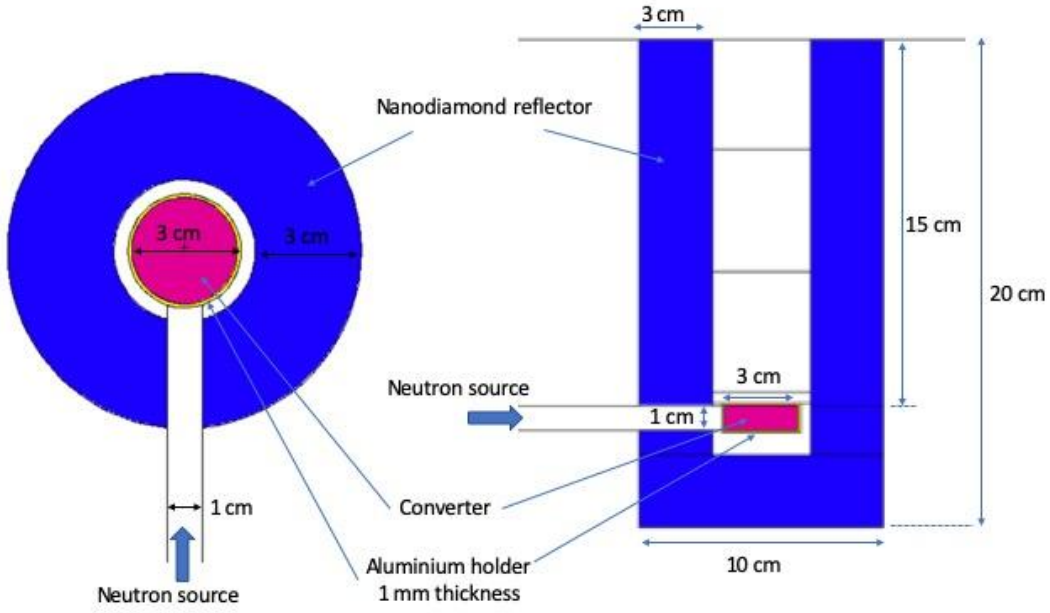

Figure 14. Geometry of the converter-reflector system.

This project has received funding from the European Union's Horizon 2020 research and innovation programme under grant agreement No. 871072.

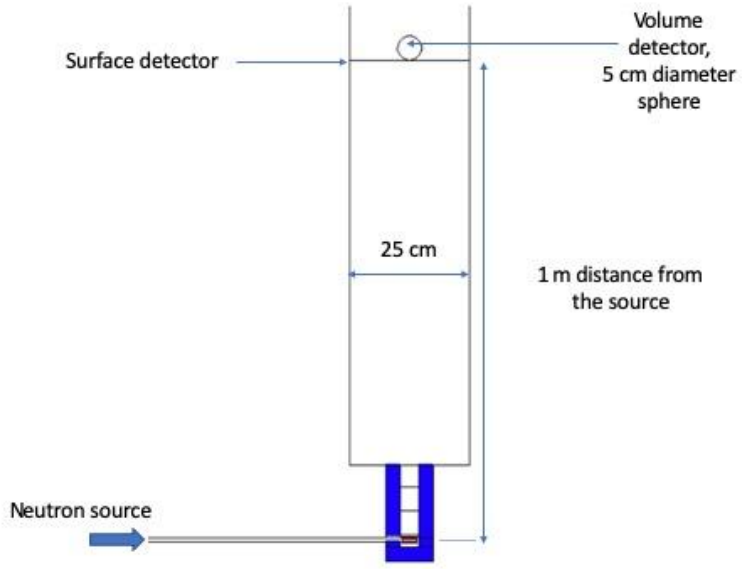

Figure 15. Geometry showing position of the tallies.

This project has received funding from the European Union's Horizon 2020 research and innovation programme under grant agreement No. 871072.

12 Figure or merit (FOM)

To define the neutron intensity [1] we start with the population of neutrons, which is described by quantity called the neutron angular density denoted by :

$$N(r, \Omega, E, t) \quad \text{(Eq. 4)}$$

and defined as the probable (or expected) number of neutrons at the position (r) with direction and energy E and at time t, per unit volume per unit solid angle per unit energy, e.g., per cm^3 per steradian per MeV. Thus

$$N(r, \Omega, E, t) dV d\Omega dE \quad \text{(Eq.5))}$$

is the expected number of neutrons in the volume element dV about r, having directions within dΩ about Ω and energies in dE about E at time t. Such a number of neutrons in an infinitesimal volume is sometimes referred to as a packet of neutrons.

Neutron angular flux which is equal to brightness in units of [$n/cm^2/s/sr/eV$] is defined as:

$$\Phi(r, \Omega, E, t) = v \cdot N(r, \Omega, E, t) \quad \text{(Eq. 6)}$$

Neutron intensity is equal to the neutron beam current:

$$I_N(E, \Omega_0, t) = \int_A v \cdot N(r, \Omega, E, t)\, da \quad \text{(Eq. 7)}$$

The following quantities were calculated:

- Neutron flux spectra, calculated using F5 point detector tallies and F4 volume detector tallies at 1 m from the source
- Neutron flux spectra using F1 surface detector tally at 16 cm from the source
- Integrated fluxes in the following wavelength ranges: between 4- 10 Å, 10-20 Å, 20-40 Å, and above 40 Å were calculated. The fluxes are normalized per source intensity (total number of source neutrons integrated through the given energy range).
- The angular distribution of the outcoming neutrons is measured at 16 cm and 1 m distance from the source beam by surface detector (F1) tally.

The intensity of the converter is proportional to the calculated flux, therefore the flux results can be used as a comparison of the different materials and geometries.

This project has received funding from the European Union's Horizon 2020 research and innovation programme under grant agreement No. 871072.

13 Results: Intensity from a bare converter

In Table 3, 4 and 5 the fluxes per source neutrons are reported. To get intensity in neutrons/source neutrons/sr, the fluxes in neutrons/source neutrons/cm^2 need to me multiplied by the area of the emission surface, and divided by the solid angle. E.g. in case of 3 cm diameter the emission surface is $\pi \cdot 1.5^2$, and in case of 1 m distance the solid angle is $\pi \cdot 1.5^2/100^2$. Therefore the factor to convert the fluxes in Tables 3,4 and 5 to intensity in neutrons/source neutrons/sr is 10^4.

Table 3. Neutron flux for different bare converter materials. Neutron flux/cm^2/source neutron at 1 m from the source detected by F5 point detector tally. Two sets of data are presented:flux for best configuration, which is chosen from the color maps of flux shown in the Appendix, and flux from a small converter size with 3 cm diameter, 1 cm high converter (most likely dimension for the prototype experiment)

Best configuration	Neutron flux/source neutrons [neutrons/source neutrons/cm^2]				
material	2-4 Å	4-10 Å	10-20 Å	20-40 Å	**> 40 Å**
Solid paradeuterium (D=100 cm, h=50 cm)	2.44E-06	3.90E-06	5.99E-07	7.84E-08	**1.04E-08**
Solid orthodeuterium (D=100 cm, h=50 cm)	5.94E-07	3.64E-06	6.32E-07	8.44E-08	**1.19E-08**
Liquid parahydrogen (D=30 cm, h= 1cm)	2.98E-06	3.00E-06	1.20E-07	1.41E-08	**1.94E-09**
Liquid orthohydrogen (D=10 cm, h=1 cm)	4.87E-06	5.52E-06	4.85E-07	2.95E-08	**1.43E-09**
Solid methane (D=14 cm, h=1 cm)	3.44E-06	5.35E-06	4.28E-07	2.32E-08	**1.3E-09**
3 cm diameter, 1 cm height	2-4 Å	4-10 Å	10-20 Å	20-40	**40 Å <**
Solid paradeuterium	7.33E-07	4.88E-07	4.37E-08	4.94E-09	**6.05E-10**
Solid orthodeuterium	6.77E-07	5.21E-07	4.82E-08	5.49E-09	**6.89E-10**
Liquid parahydrogen	6.67E-07	9.56E-07	4.47E-08	4.99E-09	**5.96E-10**
Liquid orthohydrogen	4.27E-06	5.00E-06	4.51E-07	2.53E-08	**1.60E-09**
Solid methane	3.20E-06	4.93E-06	3.98E-07	2.10E-08	**1.57E-09**
Statistical uncertainty	**<1 %**	**<1 %**	**<1 %**	**<1 %**	**<1 %**

This project has received funding from the European Union's Horizon 2020 research and innovation programme under grant agreement No. 871072.

Table 3 summarizes the most important results of flux from bare converters. The results are extracted from the color maps showing in Figure 18-22 and in the Appendix. We have summarized the results in two groups: results from the best configuration, i.e. for the dimensions of the converter that gives the highest intensity, and results for a small converter, of 3 cm diameter, 1 cm height. This is intended to give an idea of the expected performance if a small converter is used in the ILL experiment.

Table 4 The effect of the holder material and thickness on the results

3 cm diameter, 1 cm height	Neutron flux/source neutrons [neutrons/source neutrons/cm^2]				
material	2-4 Å	4-10 Å	10-20 Å	20-40 Å	**> 40 Å**
Solid orthodeuterium, 1 mm	6.77E-07	5.21E-07	4.82E-08	5.49E-09	**6.89E-10**
Solid orthodeuterium, 30 µm aluminium holder	6.44E-07	4.61E-07	4.10E-08	5.12E-09	**7.57E-10**
Solid orthodeuterium, 1 mm beryllium holder at 20 K	8.69E-07	4.42E-07	4.01E-08	5.03E-09	**7.43E-10**
Solid paradeuterium, 1 mm aluminium holder	7.48E-07	4.23E-07	3.59E-08	4.45E-09	**6.30E-10**
Solid paradeuterium, 30 µm aluminium holder	7.00E-07	4.27E-07	3.65E-08	4.56E-09	**6.69E-10**
Solid paradeuterium, 1 mm beryllium holder at 20 K	9.26E-07	4.11E-07	3.57E-08	4.47E-09	**6.67E-10**
Statistical uncertainty	<1 %	<1 %	<1 %	<1 %	**<1 %**

Most of the calculations were carried out by using 1 mm aluminium holder. As shown in Table 4, we compared the flux for a small converter, for a 30 mm Al holder and 1 mm cold holder. This has an effect of about 10% increase in the very cold neutron range.

Therefore, in the following calculations 30 µm aluminium holder was used in case of deuterium.

This project has received funding from the European Union's Horizon 2020 research and innovation programme under grant agreement No. 871072.

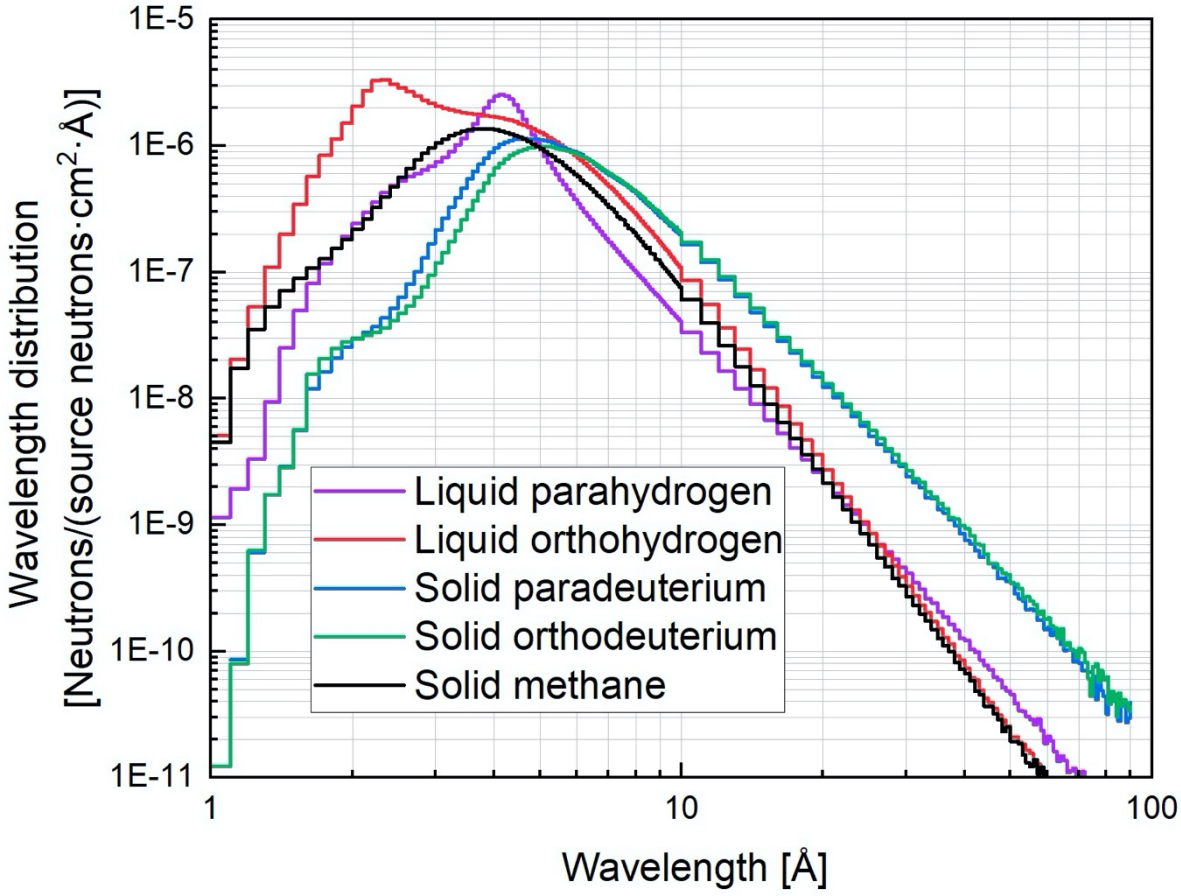

Figure 16. Spectra of best configuration as defined in Table 3.

1 m from the source detected by F5 point detector tally

This project has received funding from the European Union's Horizon 2020 research and innovation programme under grant agreement No. 871072.

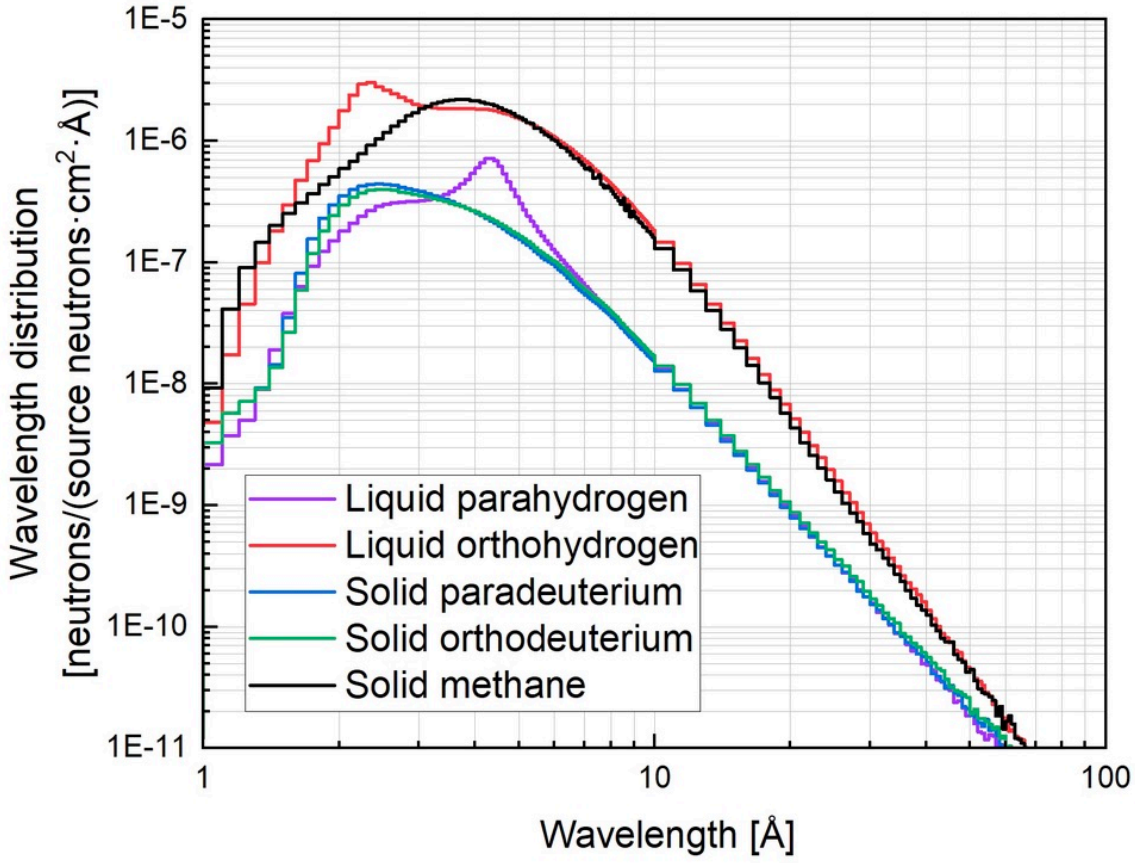

Figure 17. Spectra of 3 cm diameter, 1 cm height converter, at 1 m from the source detected by F5 point detector tally

In Figure 16 the spectra for "ideal" size converters are shown, while in Figure 17 the spectra for the small converter size are shown. The spectra are calculated above the converter as shown in Figure 13. It is interesting to see the shift in the spectra maxima. One interesting feature is the peak at about 4 Å for parahydrogen. which is not observed in typical parahydrogen spectra from moderators at spallation sources, see for instance [36]. Such shift is due to the different incoming spectrum on the converter, which is a cold spectrum, as opposed to a thermal spectrum in spallation sources or reactors.

For a VCN source, the interesting part of the spectrum is the part above 10 Å. The intensity from solid deuterium is about 1 order of magnitude higher than from the other materials, for large sizes of converters. However in the case of the small converter the hydrogen and methane converters has bigger gain in the VCN range.

This project has received funding from the European Union's Horizon 2020 research and innovation programme under grant agreement No. 871072.

13.1 Solid orthodeuterium at 5 K

In Figure 18, and in the following figures up to Figure 22, 2-dimensional maps of integrated neutron flux above 40 Å, for different converter materials, as a function of the converter diameter and height, are shown.

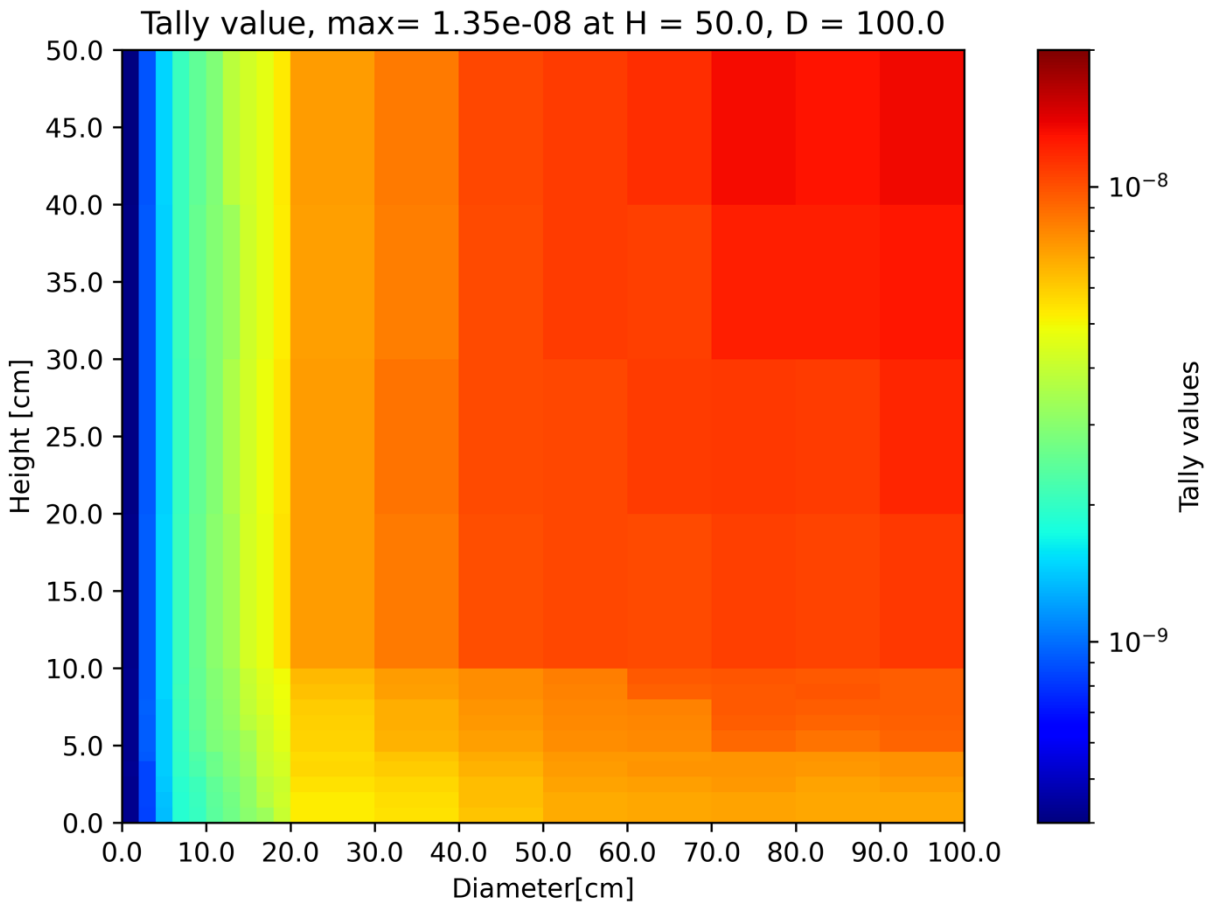

Figure 18. Neutron flux map for solid orthodeuterium, for neutrons above 40 Å, at 1 m from the source detected by F5 point detector tally [neutrons/source neutrons/cm^2]

In the case of orthodeuterium, the maximum gain was given by the largest sized converter (see Figure 18), due to its long neutron mean free path in the very cold neutron energy range (see Figure 11 and 12).

This project has received funding from the European Union's Horizon 2020 research and innovation programme under grant agreement No. 871072.

13.2 Solid paradeuterium at 5 K

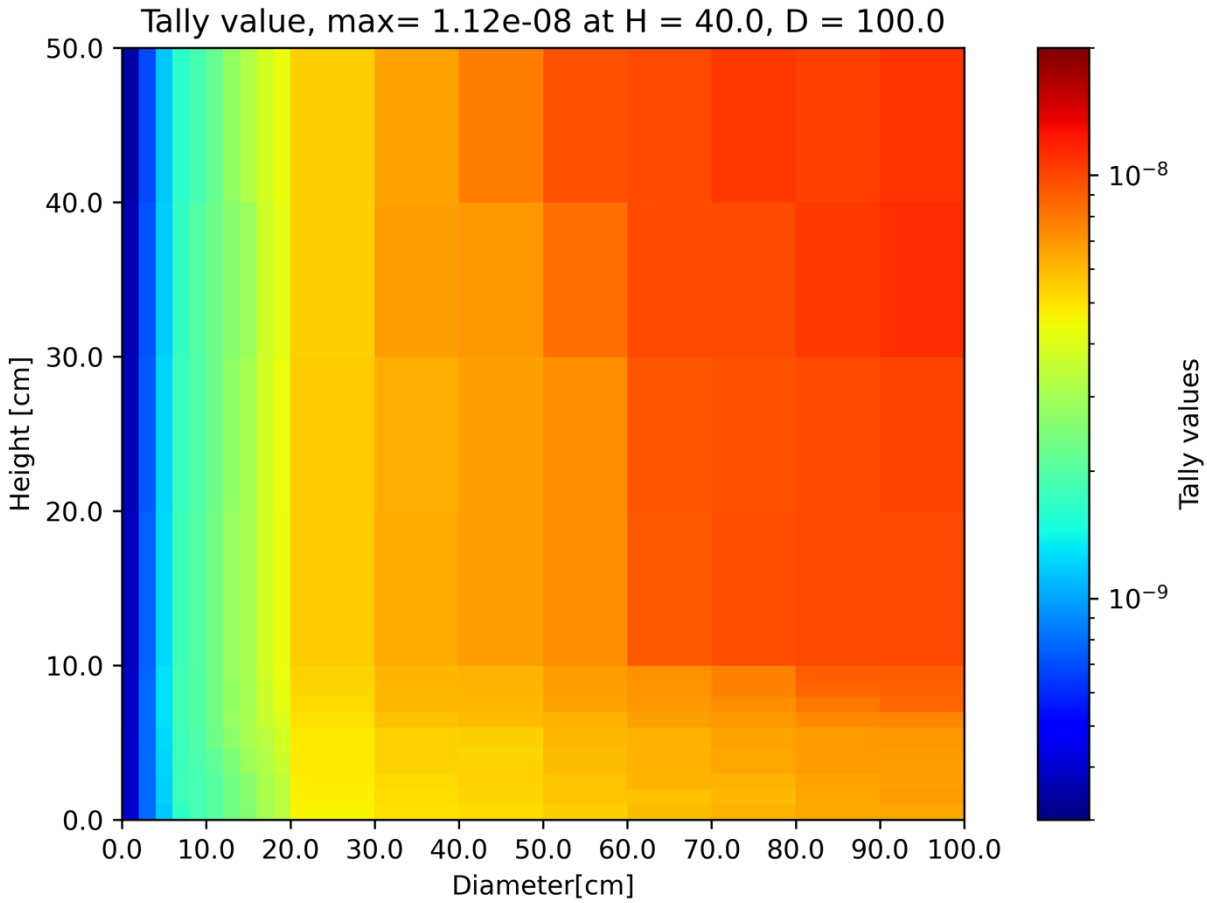

Figure 19. Neutron flux map for solid paradeuterium, for neutrons above 40 Å, at 1 m from the source detected by F5 point detector tally [neutrons/source neutrons/cm^2]

Similarly to the orthodeuterium, in the case of paradeuterium, the maximum gain was given by the largest sized converter (see Figure 19), due to its long neutron mean free path in the very cold neutron energy range (see Figure 11 and 12).

This project has received funding from the European Union's Horizon 2020 research and innovation programme under grant agreement No. 871072.

13.3 Liquid Parahydrogen at 20 K

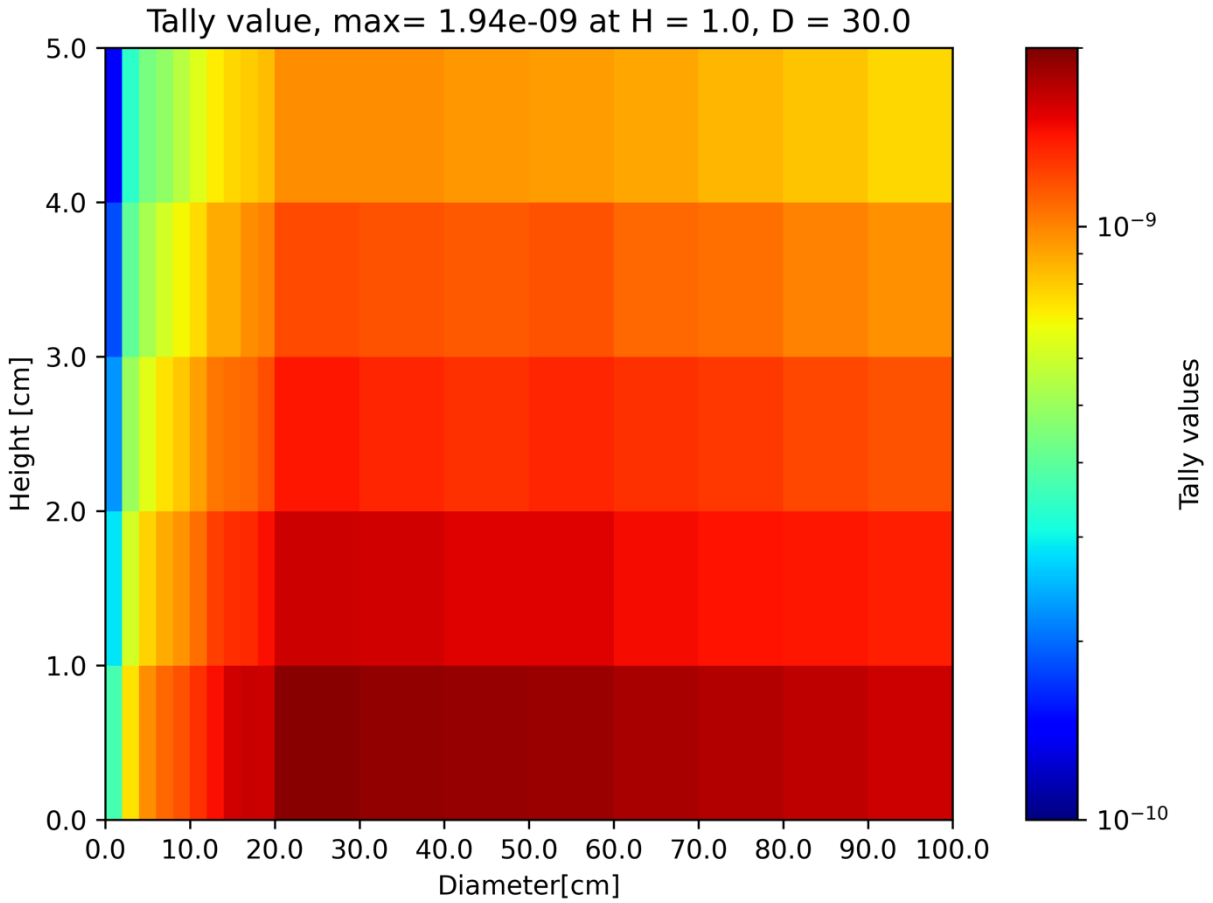

Figure 20. Neutron flux map for liquid parahydrogen, for neutrons above 40 Å, at 1 m from the source detected by F5 point detector tally [neutrons/source neutrons/cm^2]

In case of parahydrogen, the maximum gain was given by a 30 cm diameter converter (see Figure 20). The parahydrogen has around 1 centimeter mean free path in the very cold neutron energy range (see Figure 11 and 12).

This project has received funding from the European Union's Horizon 2020 research and innovation programme under grant agreement No. 871072.

13.4 Liquid orthohydrogen at 20 K

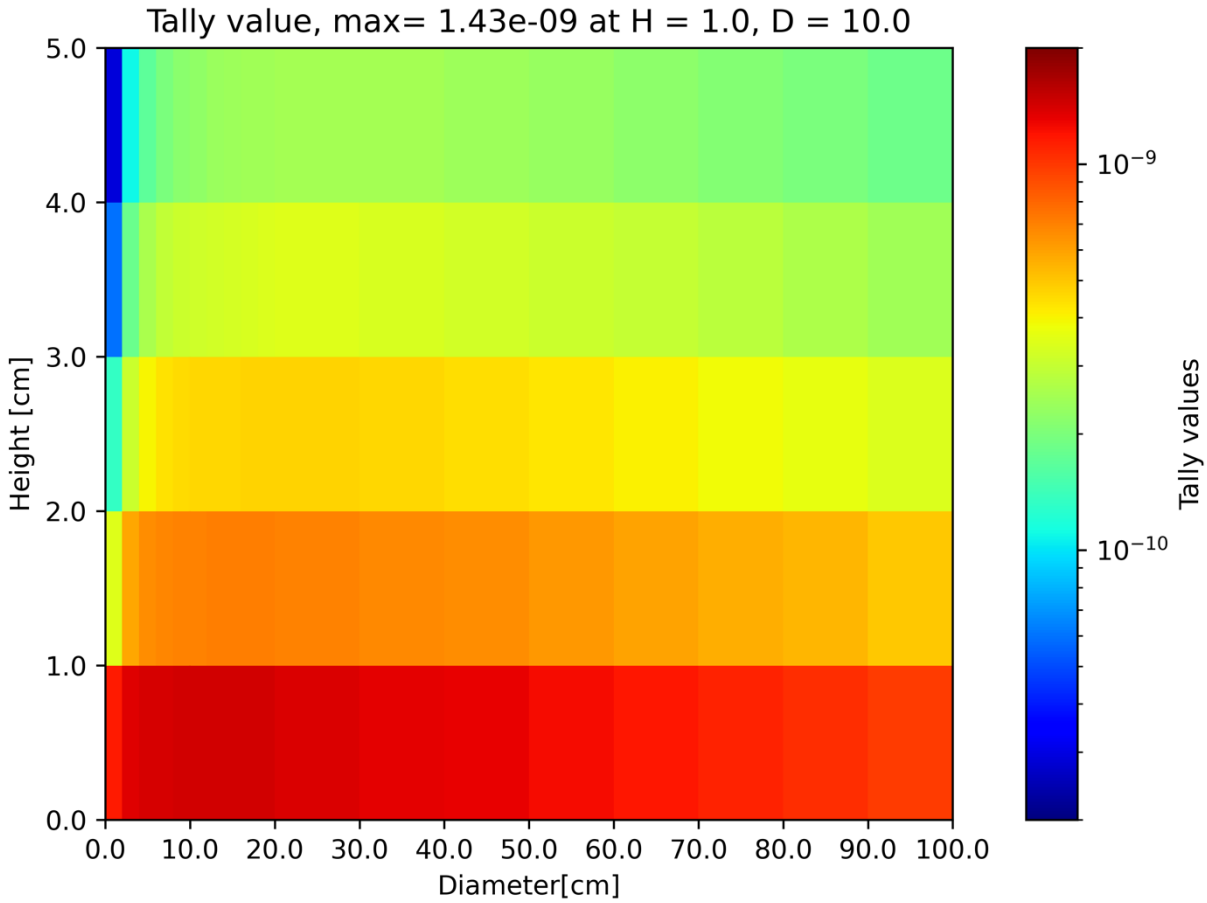

Figure 21. Neutron flux map for liquid orthohydrogen, for neutrons above 40 Å, at 1 m from the source detected by F5 point detector tally [neutrons/source neutrons/cm^2]

In the case of orthohydrogen, the maximum gain was given by a 10 cm diameter converter (see Figure 21). The orthohydrogen has about 1 mm mean free path in the very cold neutron energy range (see Figure 12).

This project has received funding from the European Union's Horizon 2020 research and innovation programme under grant agreement No. 871072.

13.5 Solid methane at 22 K

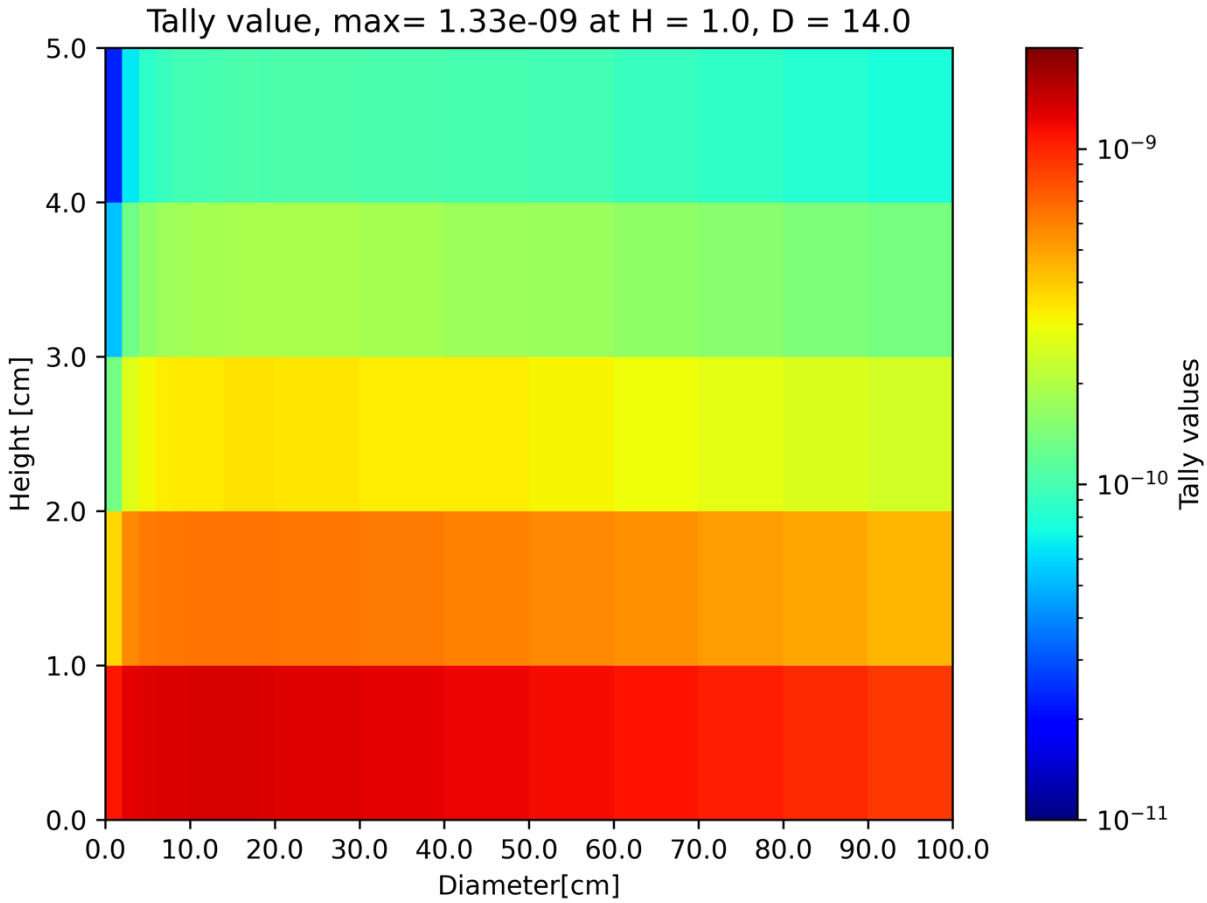

Figure 22. Neutron flux map for solid methane, for neutrons above 40 Å, at 1 m from the source detected by F5 point detector tally [neutrons/source neutrons/cm^2]

In the case of methane, the maximum gain was given by a 14 cm diameter converter (see Figure 22). The methane has about 1 mm mean free path in the very cold neutron energy range (see Figure 11 and 12).

This project has received funding from the European Union's Horizon 2020 research and innovation programme under grant agreement No. 871072.

14 Results: Intensity from a moderator/reflector system

The geometry for this case is shown in Figure 14. Table 5 summarizes the most important results from different converter materials surrounded by a nanodiamond reflector. Integral fluxes below 10 Å, above 10 Å, above 20 Å, and above 40 Å were calculated. The fluxes are normalized per source intensity (total number of source neutrons integrated through the given energy range). The solid deuterium converter surrounded by NDs gave the best flux, therefore the best intensity. For this geometry, a 5 cm diameter spherical volume detector tally (F4) was used to calculate the flux, because the F5 point detector tally was not available for calculations with nanodiamond.

Table 5 Neutron flux (neutrons/source neutrons/cm^2) for different converter materials, 3 cm diameter, 1 cm height (Tally type F4, 1 meter distance from the source)

Material	Neutron flux/source neutrons [neutrons/source neutrons/cm^2]				
	2-4 Å	4-10 Å	10-20 Å	20-40 Å	**> 40 Å**
Liquid parahydrogen+NDs	1.72E-06	1.43E-06	7.64E-08	1.17E-08	**1.92E-09**
Liquid orthohydrogen+NDs	5.11E-06	6.34E-06	4.03E-07	2.42E-08	**1.81E-09**
Solid paradeuterium+NDs	2.95E-06	2.84E-06	4.94E-08	8.14E-09	**2.63E-09**
Solid orthodeuterium+NDs	3.15E-06	3.09E-06	1.21E-07	1.22E-08	**3.16E-09**
Solid methane+NDs	4.31E-06	6.38E-06	3.45E-07	2.23E-08	**2.14E-09**
Solid methane+mirror	3.75E-06	4.30E-06	2.57E-07	1.56E-08	**1.18E-09**
Statistical uncertainty	0.30%	1%	3%	10%	**25%**

This project has received funding from the European Union's Horizon 2020 research and innovation programme under grant agreement No. 871072.

Table 6 Gain from nanodiamond reflector for different converter materials, 3 cm diameter, 1 cm height (Tally type F4, 1 meter distance from the source)

Gain from nanodiamond/mirror	2-4 Å	4-10 Å	10-20 Å	20-40 Å	**> 40 Å**
Liquid parahydrogen+NDs	1.4	1.4	1.4	0.8	**3.5**
Liquid orthohydrogen+NDs	1.3	1.4	1.1	1.2	**2.0**
Solid paradeuterium+NDs	1.8	3.2	2.5	1.8	**3.1**
Solid orthodeuterium+NDs	1.1	1.5	1.4	2.1	**4.0**
Solid methane+NDs	1.2	1.5	1.4	1.5	**2.0**
Solid methane+mirror	1.0	1.1	1.1	1.1	**1.1**

Table 7 Neutron counts (neutrons/source neutrons) for different converter materials, 3 cm diameter, 1 cm height (Tally type F1, 16 cm distance from the source)

Material	Neutron counts/ source neutrons [neutrons/source neutrons]			
	4-10 Å	10-20 Å	20-40 Å	**40 Å <**
Liquid parahydrogen+NDs	5.79E-04	6.06E-05	1.67E-05	**6.04E-06**
Liquid orthohydrogen+NDs	2.82E-03	4.23E-04	4.63E-05	**7.39E-06**
Solid paradeuterium+NDs	1.35E-03	6.95E-05	2.26E-05	**1.53E-05**
Solid orthodeuterium+NDs	1.43E-03	1.46E-04	2.53E-05	**1.61E-05**
Solid methane+NDs	2.81E-03	3.66E-04	4.35E-05	**8.51E-06**
Solid methane+mirror	2.30E-03	1.76E-04	2.73E-05	**5.81E-06**
Statistical uncertainty	0.1%	<0.2%	<1%	**<2%**

This project has received funding from the European Union's Horizon 2020 research and innovation programme under grant agreement No. 871072.

Table 8 Gain from nanodiamond reflector for different converter materials, 3 cm diameter, 1 cm height (Tally type F1, 16 cm distance from the source)

Gain from nanodiamond/mirror	4-10 Å	10-20 Å	20-40 Å	**> 40 Å**
Liquid parahydrogen+NDs	1.1	2.1	4.7	**13.8**
Liquid orthohydrogen+NDs	1.2	2.7	4.8	**12.7**
Solid paradeuterium+NDs	5.6	3.8	9.2	**44.2**
Solid orthodeuterium+NDs	1.2	3.1	9.7	**44.2**
Solid methane+NDs	1.2	2.7	5.1	**14.1**
Solid methane+mirror	1.0	1.3	3.2	**9.6**

At the exit of the ND reflector an increase by a factor of 44 was computed when using the deuterium converter, an increase by a factor of 13-14 was observed when hydrogen converter was used, while an increase by a factor of 14 was calculated when the converter material was methane. These gains were computed considering neutrons 40 Å <. Most of this gain is due to high-divergence neutrons.

The angular distribution show that most of the increase is due to high-divergence neutrons. Therefore, this increase can be measured only at the exit of the nanodiamond reflector.

For low-divergence neutrons, at 1 m from the source an increase by a factor of 3 was predicted when using the paradeuterium converter, an increase by a factor of 4 was observed when orthodeuterium converter was used, an increase by a factor of 3.5 was computed when the converter material was parahydrogen, while an increase by a factor of 2 was calculated when using orthohydrogen or methane converters. At 1 m from the source, the neutron flux was calculated inside a 5 cm diameter spherical volume detector tally (the solid angle is 3 degree). This result is quite interesting because these are low divergence neutrons, usable in neutron scattering experiments. We would expect to observe such a gain in the prototype experiment.

As a comparison with NDs, we considered a similar geometry where supermirrors with m=6 replace the NDs. With a methane converter, an increase by a factor of 10 was predicted at 16 cm from the

This project has received funding from the European Union's Horizon 2020 research and innovation programme under grant agreement No. 871072.

source, but only 10 % gain was observed at 1 m from the source. It is because neutron mirrors work well in different geometries, e.g. as a neutron guide.

This project has received funding from the European Union's Horizon 2020 research and innovation programme under grant agreement No. 871072.

15 Differential cross section of para- and othodeuterium

The difference between ortho- and paradeuterium is due to upscattering in paradeuterium. To test this we simulated the same geometry (Figure 14-15), replacing the beam by a 40 Å monoenergetic neutron beam (Figure 23). This additional upscattering can be observed (Figure 24) in the energy differential cross section for 40 Å, which shows the same features at low energy, with an additional scattering probability for outgoing energies in the 1-10 meV range for paradeuterium.

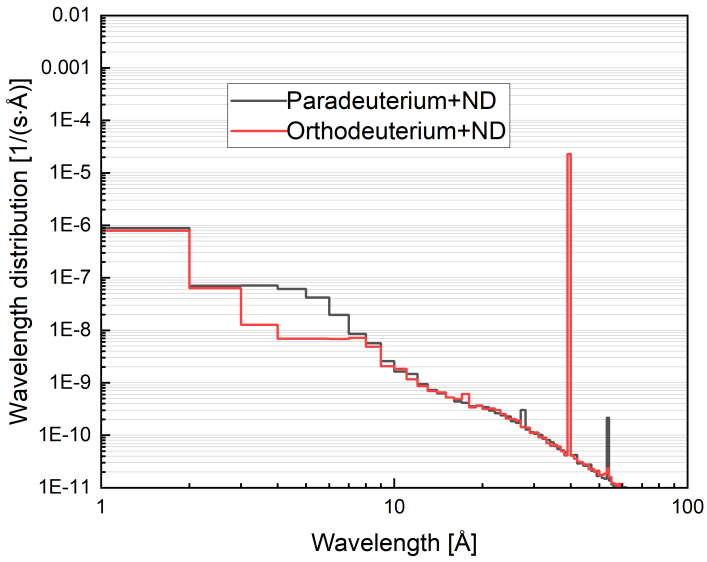

Figure 23. Neutron spectra at 1 m F4 volume detector tally, 5 cm diameter sphere for a monoenergetic 40 A beam.

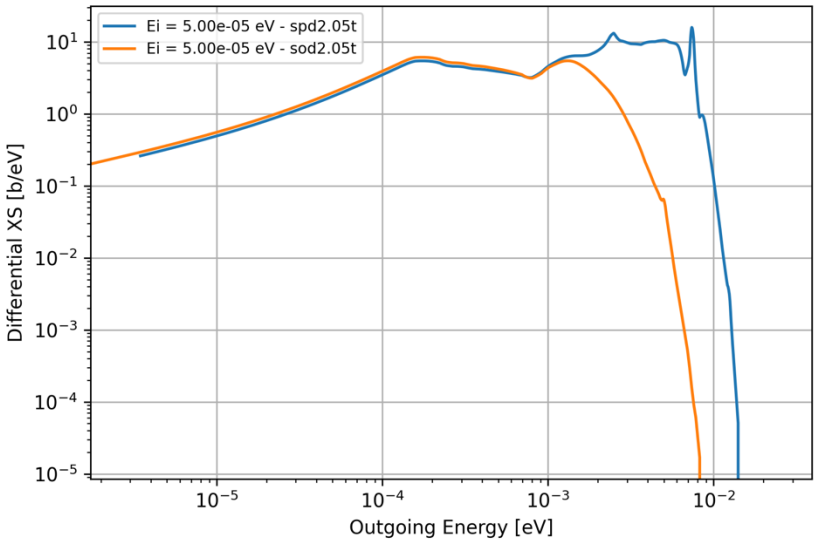

Figure 24 Differential cross section of para- and orthodeuterium at 40 Å

This project has received funding from the European Union's Horizon 2020 research and innovation programme under grant agreement No. 871072.

16 Effect of elastic and inelastic cross section

Since the incident spectrum at PF1B is already cold, there is a VCN tail that would be dispersed by the elastic cross section of solid converter materials, in addition to the inelastic downscattering effect. To quantify this we computed the in-scattering probability from an incident energy E_i to an outgoing energy $E_f < 0.05$ meV (equivalent to 40 Å), and multiplied it by the inelastic cross section at E_i to obtain the cross section of VCN production by single scattering. This cross section, integrated over the incident spectrum, gives the VCN production rate from single scattering events.

$$R_{inel} = \int_0^{\infty} dE_i \, \Phi(E_i)\sigma_{inel}(E_i)p\left(E_i \rightarrow E_f < 0.05\ meV\right) \quad \text{(Eq.4)}$$

This can be compared to the dispersion of VCNs, computed as the integral over the spectrum for $E_i <$ 0.05 meV times the elastic cross section at E_i.

$$R_{el} = \int_0^{0.05\ meV} dE_i \, \Phi(E_i)\sigma_{el}(E_i) \quad \text{(Eq. 5)}$$

The results, normalized to the total number of events, are shown in Table 8.

Table 9 Elastic and inelastic scattering part in different converters

	Inelastic part	Elastic part
Solid orthodeuterium	88%	12%
Solid paradeuterium	75%	25%
Solid methane	66%	34%

Although the contribution of neutrons dispersed by elastic scattering is not negligible, the majority of the VCN neutrons are produced by inelastic events. It is important to note that this analysis is simplified because it does not include the production of VCNs by multiple scattering events.

This project has received funding from the European Union's Horizon 2020 research and innovation programme under grant agreement No. 871072.

17 Results: Angular distribution of a moderator/reflector system

The angular distribution of the outcoming neutrons is calculated at 16 cm (at the exit of the reflector) and 1 m distance from the source beam by surface detector (F1) tally shown in Figure 25-28. The gain from the nanodiamond converter is more visible at high angles, while most of the gain is lost at 1 m distance, where only small angle neutrons arrive.

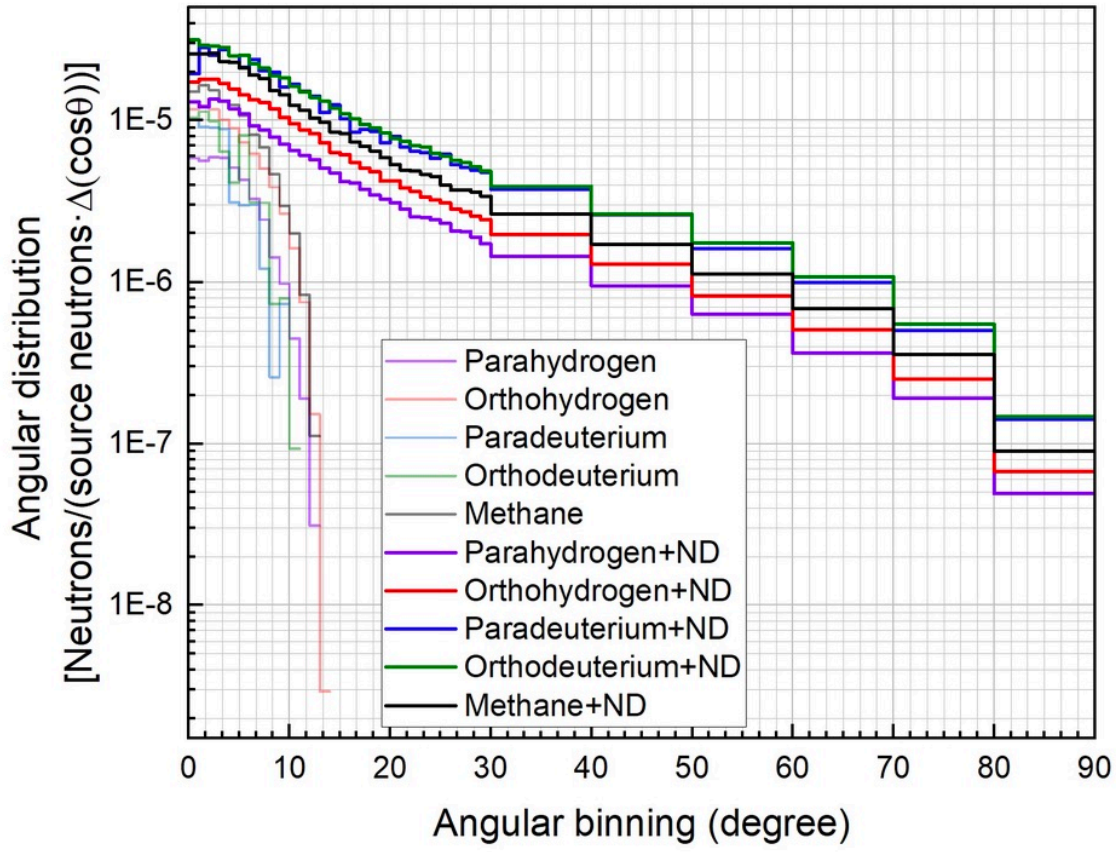

Figure 25. Angular distribution of neutrons, 40 Å <neutron wavelength, at 16 cm from the source, 12.5x12.5 cm^2 detector surface, F1 tally

Figure 25 shows the angular distribution of neutrons for different converter materials, at 16 cm from the source. It is well visible that most of the gain by the nanodiamond is due to high angle neutrons.

This project has received funding from the European Union's Horizon 2020 research and innovation programme under grant agreement No. 871072.

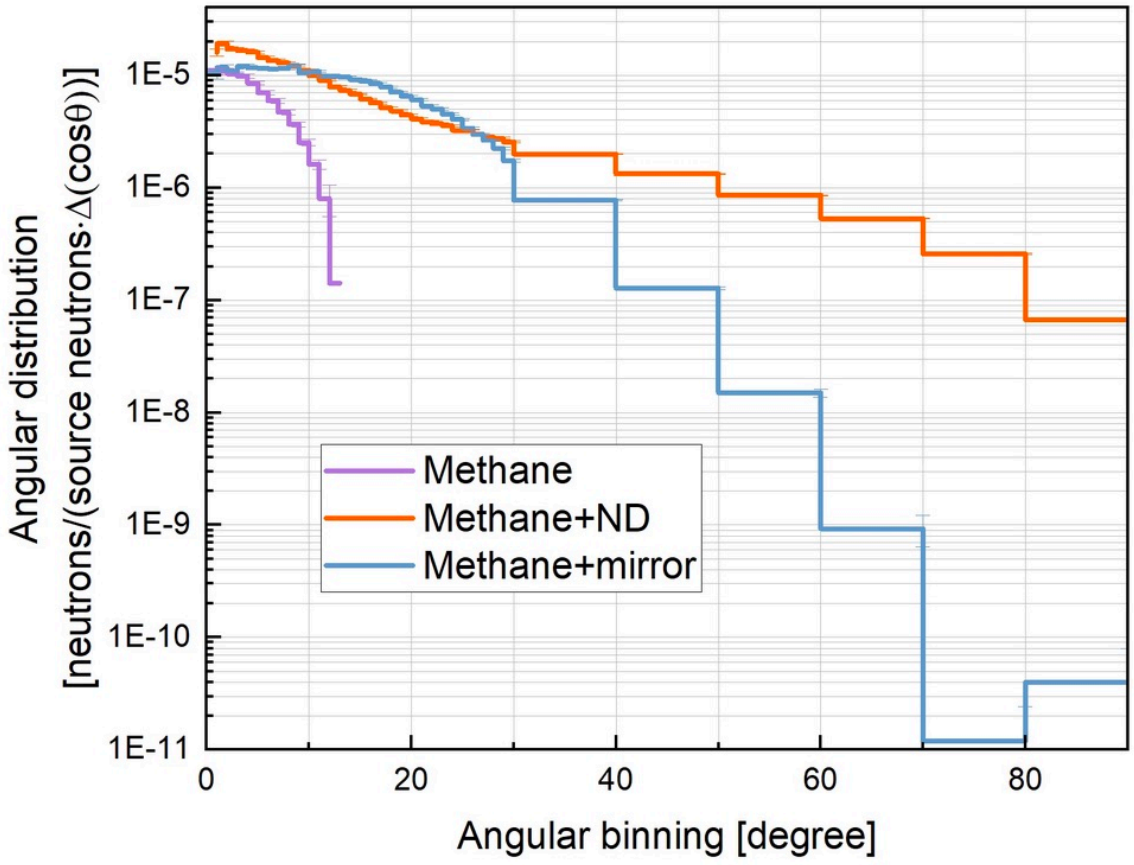

Figure 26. Angular distribution of neutrons,, 40 Å <neutron wavelength, at 16 cm from the source, 12.5x12.5 cm^2 detector surface, F1 tally

Figure 26 shows the angular distribution of neutrons for bare methane converter, methane converter surrounded by nanodiamond reflector, and methane converter surrounded by neutron mirror, at 16 cm from the source. Most of the gain by both the nanodiamond and neutron mirror is due to high angle neutrons.

This project has received funding from the European Union's Horizon 2020 research and innovation programme under grant agreement No. 871072.

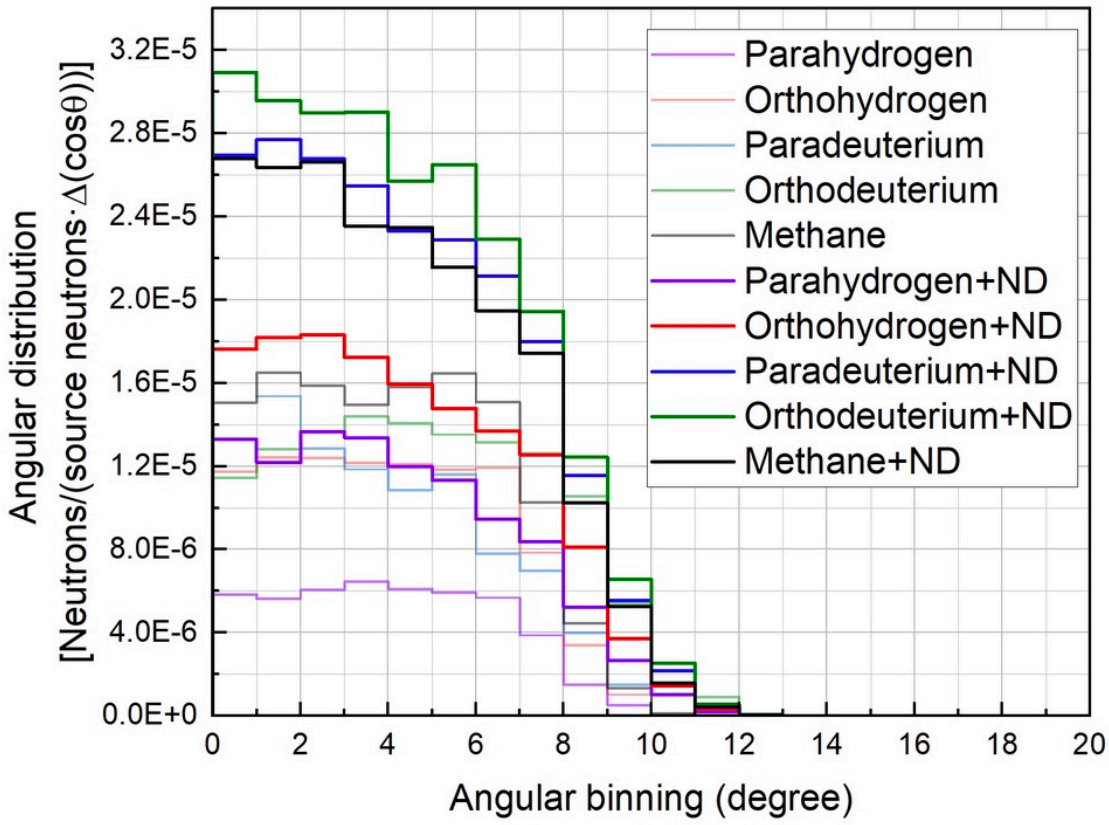

Figure 27. Angular distribution of neutrons, 40 Å <neutron wavelength, at 1 m, 25x25 cm^2 detector surface, F1 tally

Figure 27 shows the angular distribution of neutrons for different converter materials, at 1 m from the source.

This project has received funding from the European Union's Horizon 2020 research and innovation programme under grant agreement No. 871072.

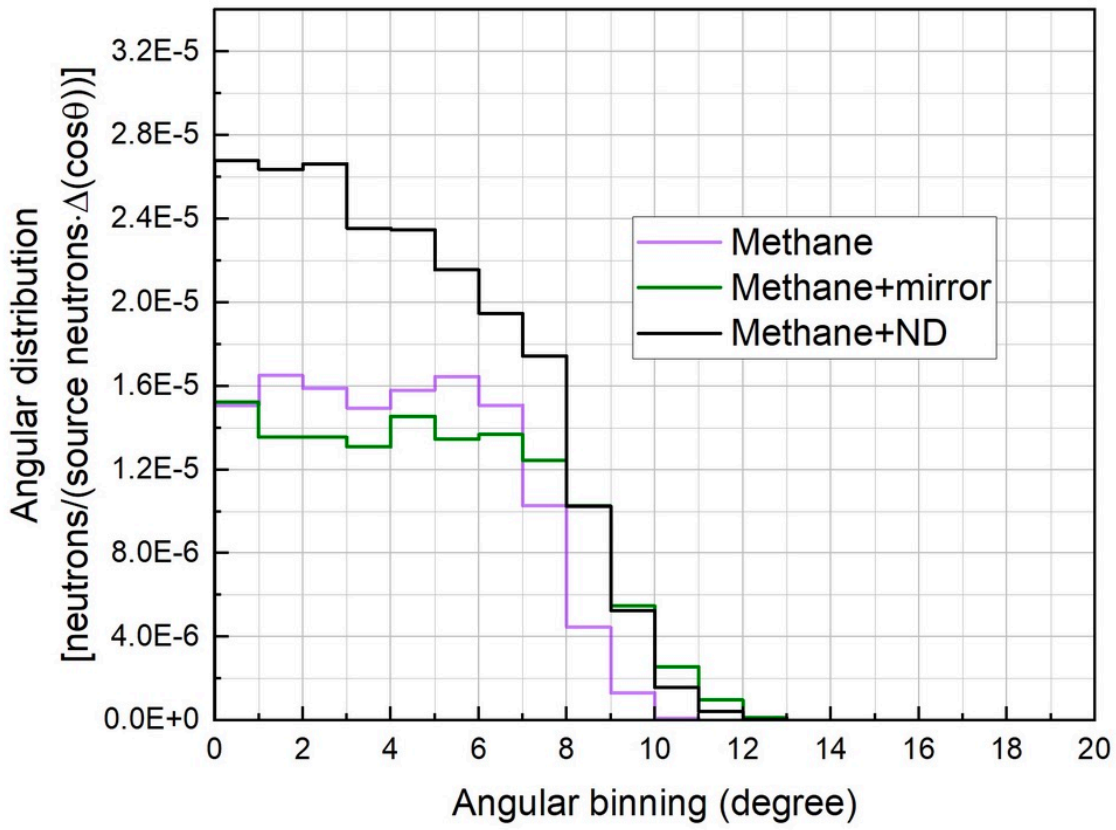

Figure 28. Angular distribution of neutrons, 40 Å < neutron wavelength, at 1 m, 25x25 cm^2 detector surface, F1 tally

Figure 28 shows the angular distribution of neutrons for bare methane converter, methane converter surrounded by nanodiamond reflector, and methane converter surrounded by neutron mirror, at 1 m from the source.

This project has received funding from the European Union's Horizon 2020 research and innovation programme under grant agreement No. 871072.

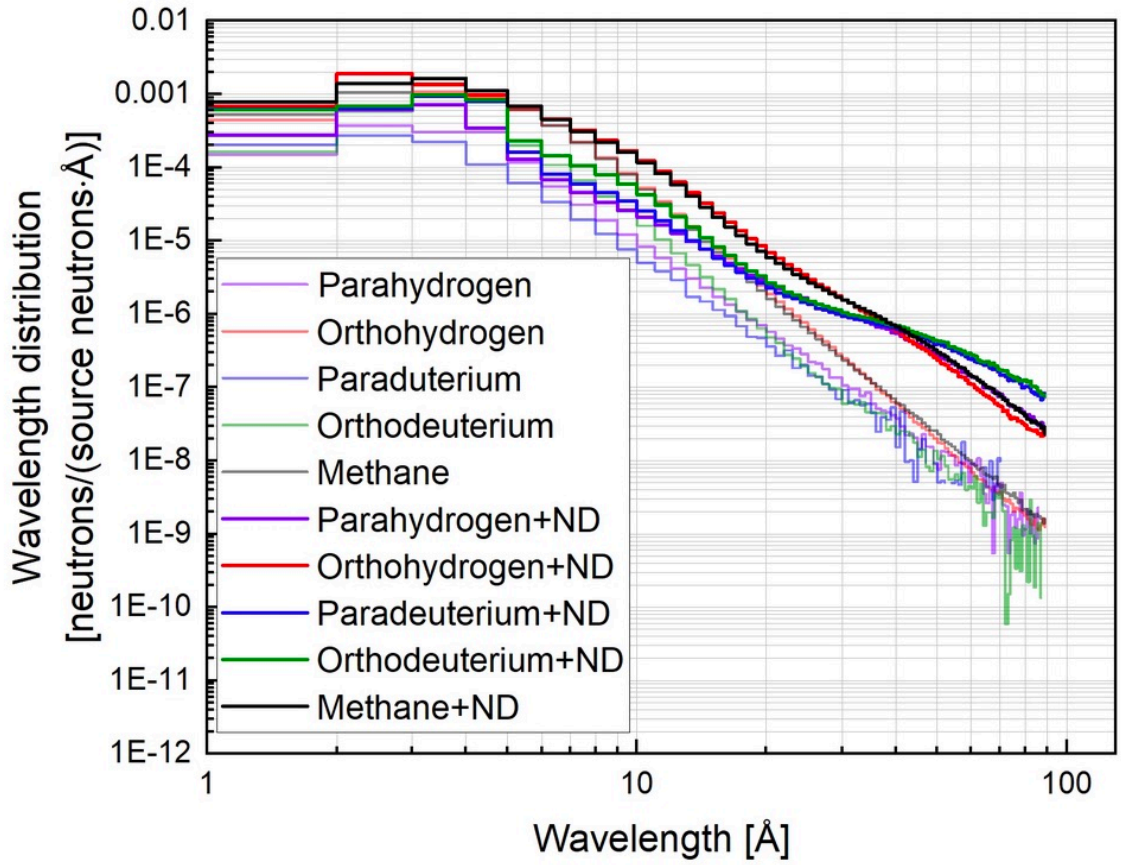

Figure 29. Neutron spectra at 16 cm, 12.5x12.5 cm^2 detector surface, F1 surface detector tally

Figure 29 shows the neutron spectra at 16 cm for different converters, the gain from nanodiamond is well visible above 20 Å.

This project has received funding from the European Union's Horizon 2020 research and innovation programme under grant agreement No. 871072.

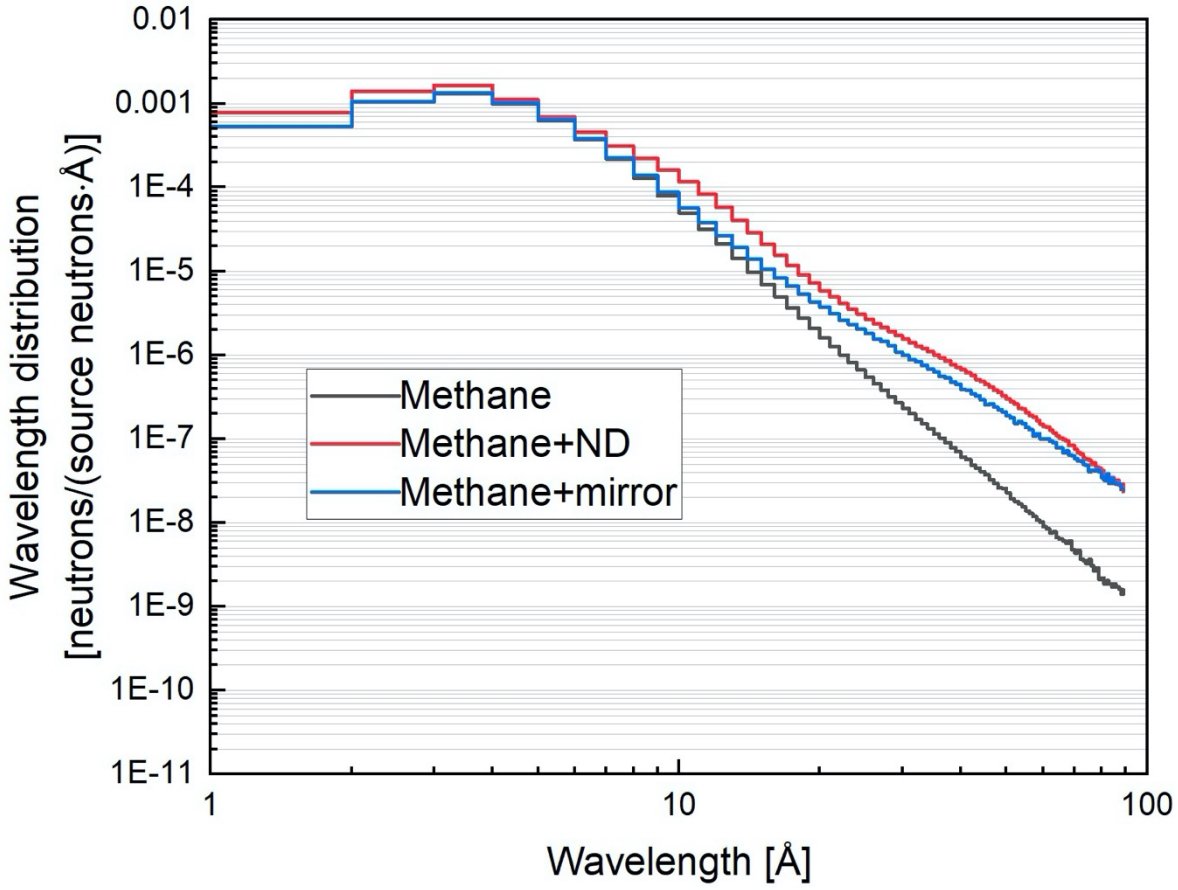

Figure 30. Neutron spectra at 16 cm, 12.5x12.5 cm^2 detector surface, F1 surface detector tally

Figure 30 shows for bare methane converter, methane converter surrounded by nanodiamond reflector, and methane converter surrounded by neutron mirror, at 16 cm from the source. Similarly to nanodiamond, the gain from neutron mirror is also well visible above 20 Å.

This project has received funding from the European Union's Horizon 2020 research and innovation programme under grant agreement No. 871072.

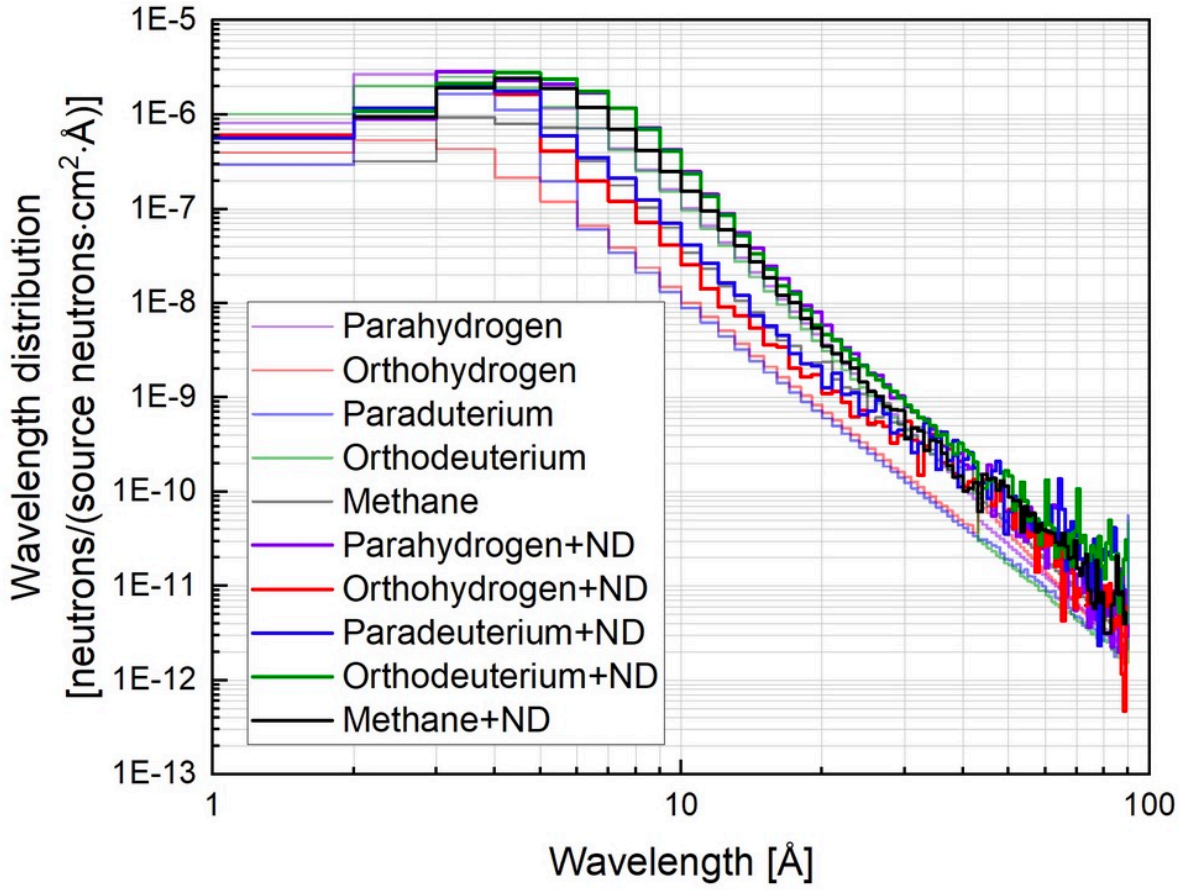

Figure 31. Neutron spectra at 1 m F4 volume detector tally

Figure 31 shows the neutron spectra at 1 m from the source for different converters, the gain from nanodiamond is less pronounced than closer to the converter.

This project has received funding from the European Union's Horizon 2020 research and innovation programme under grant agreement No. 871072.

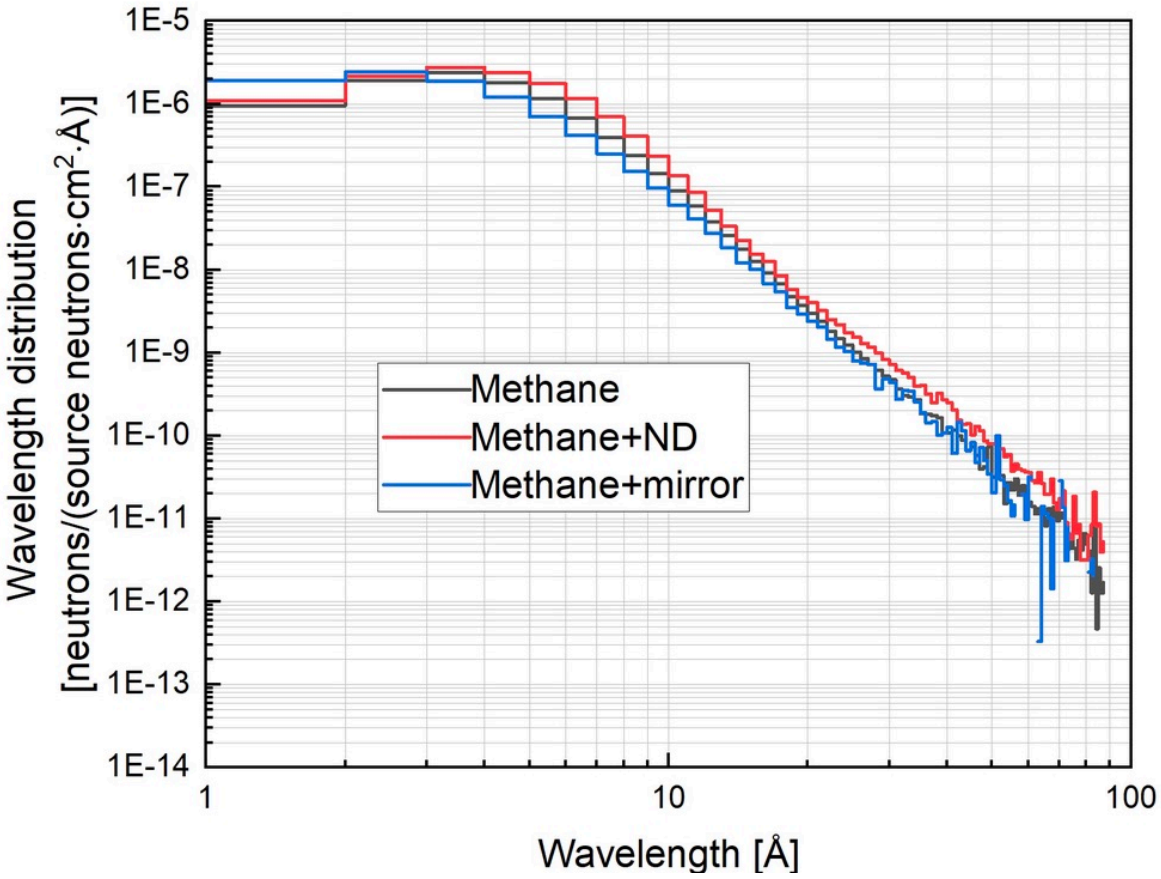

Figure 32. Neutron spectra at 1 m F4 volume detector tally

Figure 32 shows the neutron spectra at 1 m from the source for bare methane converter, methane converter surrounded by nanodiamond reflector, and methane converter surrounded by neutron mirror. Comparing with Figure 28, the effect of neutron mirror is not significant.

This project has received funding from the European Union's Horizon 2020 research and innovation programme under grant agreement No. 871072.

Figures 33-34 show the neutron intensity decreases by distance from the source. Figure 31 shows results with different converter materials and neutrons above 40 Å, while Figure 32 shows only orthodeuterium at different energy ranges. The expected inverse square decrease in flux is well visible in all graphs.

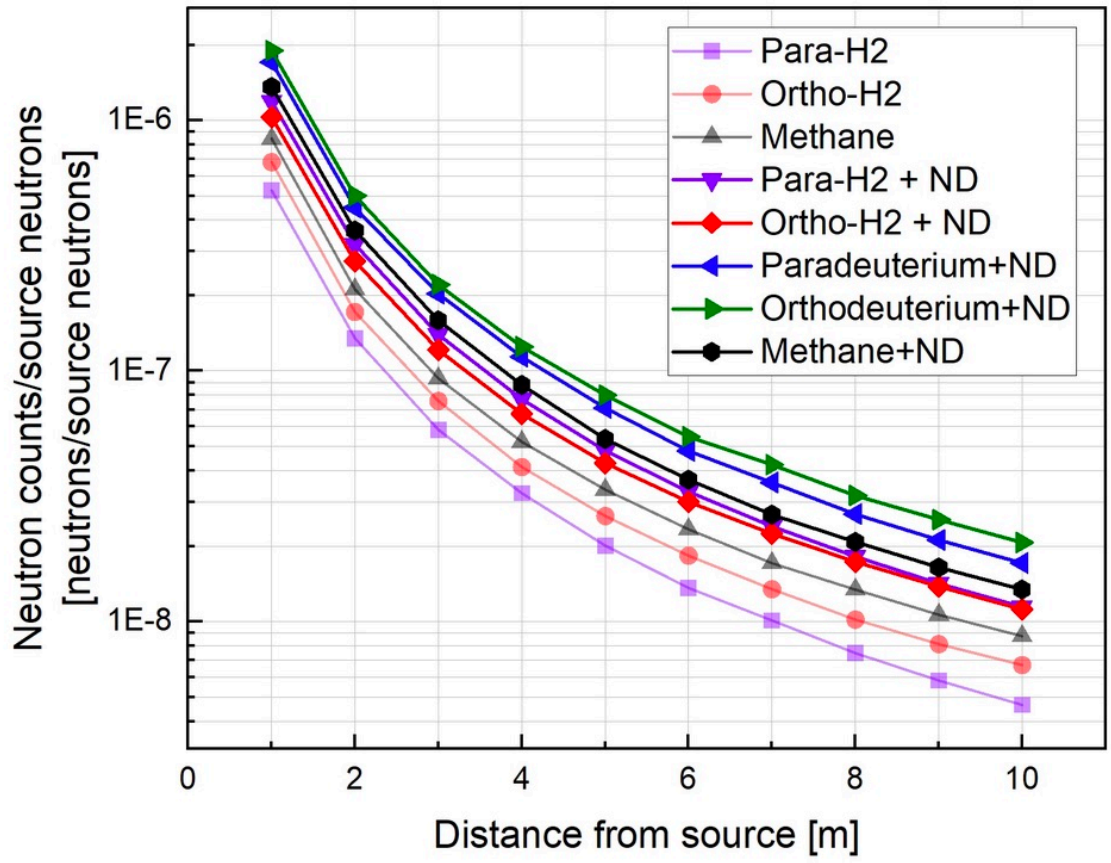

Figure 33. Neutron counts (neutrons/source neutrons) for different converter materials at different distances (3 cm diameter, 1 cm height converter, Tally type F1), neutrons above 40 Å

This project has received funding from the European Union's Horizon 2020 research and innovation programme under grant agreement No. 871072.

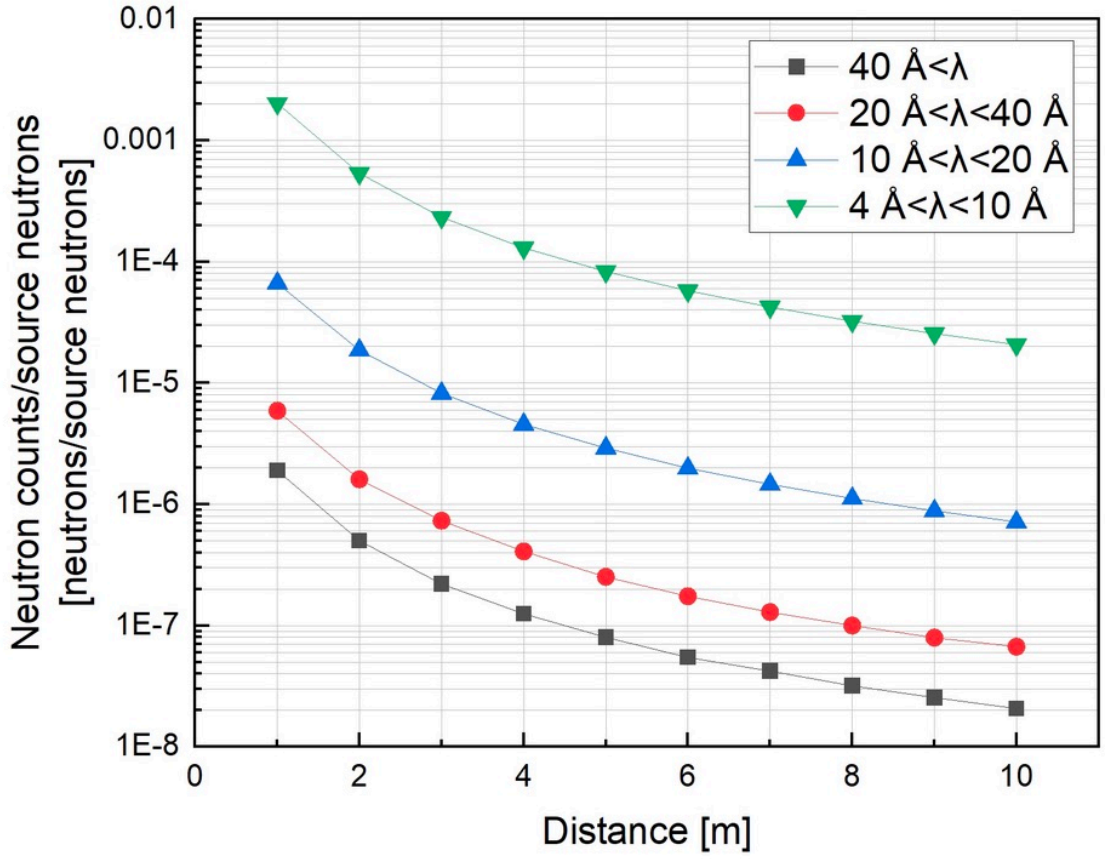

Figure 34. Neutron counts for solid orthodeuterium converter at different distances (3 cm diameter, 1 cm height converter, Tally type F1)

This project has received funding from the European Union's Horizon 2020 research and innovation programme under grant agreement No. 871072.

18 Expected count rates for prototype experiment

The neutron capture flux density of H113 is $\Phi_C = 2 \cdot 10^{10}$ n/(cm^2 s). The particle flux is 2.7 times lower than the capture flux density. The PF1B spectrum is shown in Figure 3. For the source intensity we multiplied the particle flux by the source area (1 cm diameter circle).

The neutron counts were calculated by a 25 cm x 25 cm surface detector tally (F1), at 1 m from the neutron source.

We considered that the velocity selector transmits about 8% of the initial beam.

The tally results were multiplied by $4.65 \cdot 10^8$ n/s neutron intensity in order to get the expected count rates.

Table 10 Expected count rates at 1 m from the source, 25 cm x 25 cm surface detector

	4-10 Å	10-20 Å	20-40 Å	**> 40 Å**
Material	Neutron counts/second			
Liquid parahydrogen+ND	3.70E+05	1.37E+04	2.00E+03	3.79E+02
Liquid orthohydrogen+ND	1.98E+06	1.11E+05	6.64E+03	5.31E+02
Solid paradeuterium+ND	8.90E+05	1.43E+04	2.46E+03	8.52E+02
Solid orthodeuterium+ND	9.40E+05	3.08E+04	2.74E+03	8.83E+02
Solid methane+ND	1.80E+06	9.08E+04	5.58E+03	6.27E+02
Statistical uncertainty	0.1%	0.3%	1%	2%

Based on our calculations, at 1 m from the neutron source, at the end of the reflector, the expected count rate of very cold neutrons above 40 Å is about 400 neutron per second (nps) in case of parahydrogen surrounded by nanodiamond, and about 500 nps in case of orthohydrogen surrounded by nanodiamond. The expected count rate is about 900 nps in case of deuterium surrounded by nanodiamond, and 600 nps in case of methane surrounded by nanodiamond.

This project has received funding from the European Union's Horizon 2020 research and innovation programme under grant agreement No. 871072.

19 Conclusions

A comprehensive study of the intensity of Very Cold Neutrons (VCNs) from different moderator and converter materials was performed by Monte Carlo calculations using MCNP6.2. The goal of the study was to investigate the performance of such materials to generate VCNs, and to couple such materials with a reflector of nanodiamonds, in view of a possible prototype experiment for an advanced VCN source.

The choice of candidate VCN converters was based on expectations of good performance, and on the availability of thermal scattering cross sections in ACE format to be used in MCNP. The following materials were analyzed: solid para- and orthodeuterium at 5 K, liquid para- and orthohydrogen at 14 K and solid methane at 22 K.

The calculations were carried out using the MCNP 6.2. code. A cylindrical converter was irradiated by a collimated cold neutron beam from the side. A sensitivity study was performed varying the height and diameter of the moderator: the height of the moderator was changed between 1 and 50 cm, the diameter was changed between 2 and 100 cm.

The cold neutron source was defined by the description of the beam characteristics of the first ballistic supermirror neutron guide H113 that feeds the neutron user facility for particle physics PF1B of the Institute Laue-Langevin, Grenoble (ILL), where a prototype experiment is intended to be performed.

Several important findings resulted from this work:

Results from simulation of bare converter:

1. Size of the converter: It can be concluded that the maximum gain is given by the biggest size solid deuterium converter (100 cm diameter, 50 cm height). In case of parahydrogen, the maximum gain is given by the 30 cm diameter converter. In case of orthohydrogen, the maximum gain is given by the 10 cm diameter converter. In case of methane, the maximum gain is given by the 14 cm diameter converter.
2. Difference between ortho- and paradeuterium: About 20 % higher gain is predicted by orthodeuterium converter compared to paradeuterium using the small geometry converter and 30 µm thickness aluminium holder. Orthodeuterium performs better because of its lower upscattering cross section, which increases conversion, and its higher elastic cross section which redirects VCNs already present in the incident beam.
3. Difference between converter materials: There is a clear higher output for solid deuterium, about 1 order of magnitude higher than for the other materials, for the ideal sizes of VCN

This project has received funding from the European Union's Horizon 2020 research and innovation programme under grant agreement No. 871072.

sources. Neutrons have smaller mean free path in methane and hydrogen, so their intensity cannot be increased significantly by increasing the volume of the converter.

4. In terms of the experiment configuration (3 cm diameter, 1 cm height) the liquid orthohydrogen and the solid methane converters gave higher output by a factor of 4 compared to the liquid parahydrogen and the solid deuterium converters.

Converter with reflector:

5. At the exit of the ND reflector an increase by a factor of 44 was computed when using the deuterium converter, an increase by a factor of 13-14 was observed when hydrogen converter was used, while an increase by a factor of 16 was calculated when the converter material was methane. These gains were computed considering neutrons 40 Å <. Although hydrogen and methane converters produce a higher intensity, solid deuterium produces a higher fraction of long wavelength neutrons (see Figure 17), which are most affected by the utilisation of nanodiamond.
6. The angular distribution at the exit of the ND reflector shows that most of the increase is due to high-divergence neutrons.
7. For low-divergence neutrons, at 1 m from the source an increase by a factor of 3 was predicted when using the paradeuterium converter, an increase by a factor of 4 was observed when orthodeuterium converter was used, an increase by a factor of 3.5 was computed when the converter material was parahydrogen, while an increase by a factor of 2 was calculated when using orthohydrogen or methane converters. At 1 m from the source, flux was calculated by 5 cm diameter spherical volume detector tally (the solid angle is 3 degree). This result is quite interesting because these are low divergence neutrons, usable in neutron scattering experiments. We would expect to observe such a gain in the prototype experiment.
8. As a comparison with NDs, we considered a similar geometry where supermirrors with m=6 replace the NDs. With a methane converter, a 9 times increase was predicted at 16 cm from the source, but only 10 % gain was observed at 1 m from the source.

This project has received funding from the European Union's Horizon 2020 research and innovation programme under grant agreement No. 871072.

20 Appendix A: neutron intensity from bare converters

In the Appendix intensity for different bare converter materials are shown. The tally values show the neutron flux/source neutron at 1 m from the source detected by F5 point detector tally. Each plot corresponds to different converter material and different neutron energy range. Table 3 summarizes the most important results of intensity from bare converters. The results in that table are extracted from the color maps showing in Figure 18-22 and in the Appendix.

In general it can be concluded that the maximum gain for neutrons above 4 Å was given by the biggest size solid deuterium converter (100 cm diameter, 50 cm height). In case of liquid hydrogen and solid methane, the maximum gain was given by the smallest possible height (1 cm) and by a certain diameter in dm range.

This project has received funding from the European Union's Horizon 2020 research and innovation programme under grant agreement No. 871072.

a. Solid orthodeuterium at 5 K

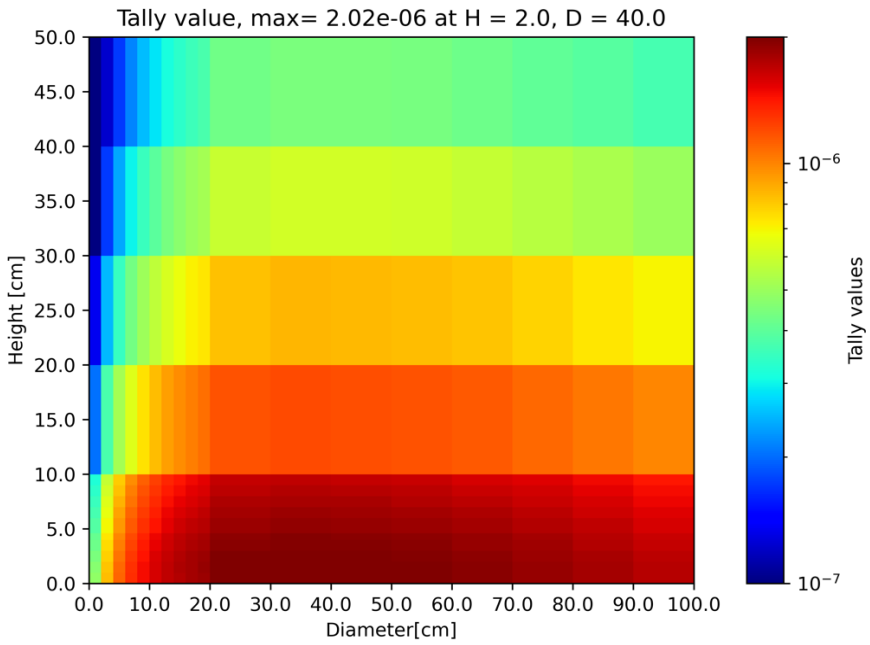

Figure 20-1 Neutron flux map for solid orthodeuterium, for neutrons between 2-4 Å [neutrons/source neutrons/cm^2]

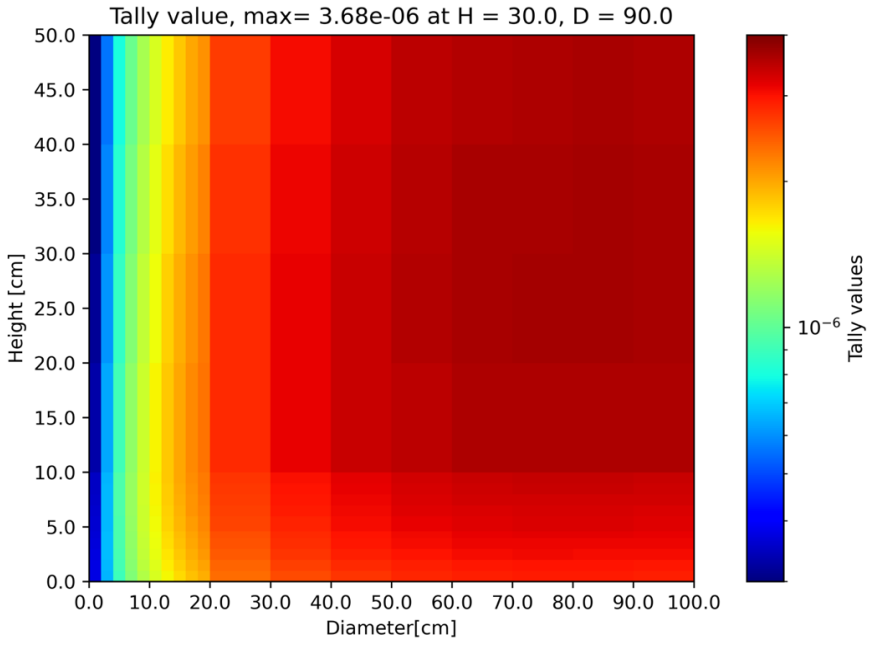

Figure 20-2 Neutron flux map for solid orthodeuterium, for neutrons between 4-10 Å [neutrons/source neutrons/cm^2]

This project has received funding from the European Union's Horizon 2020 research and innovation programme under grant agreement No. 871072.

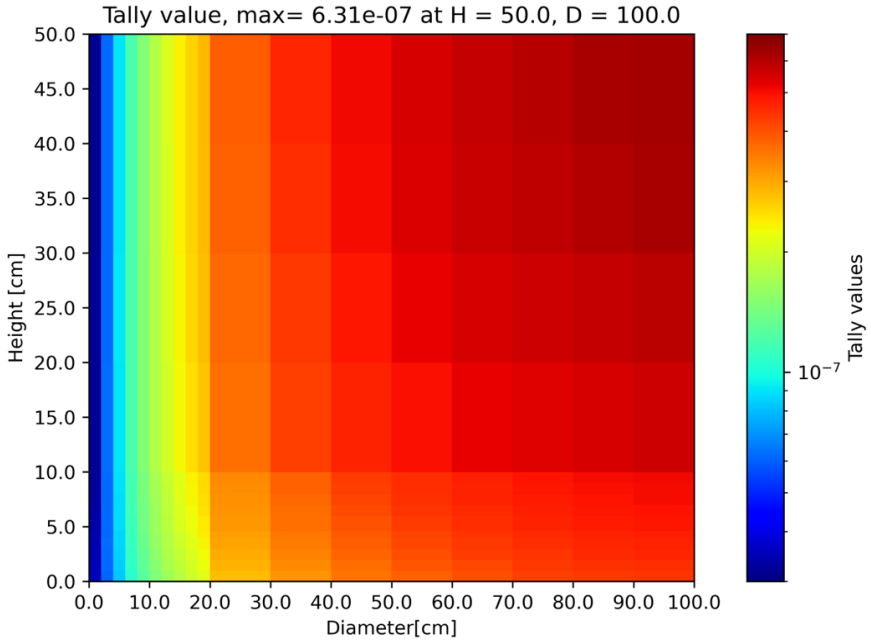

Figure 20-3 Neutron flux map for solid orthodeuterium, for neutrons between 10-20 Å [neutrons/source neutrons/ cm^2]

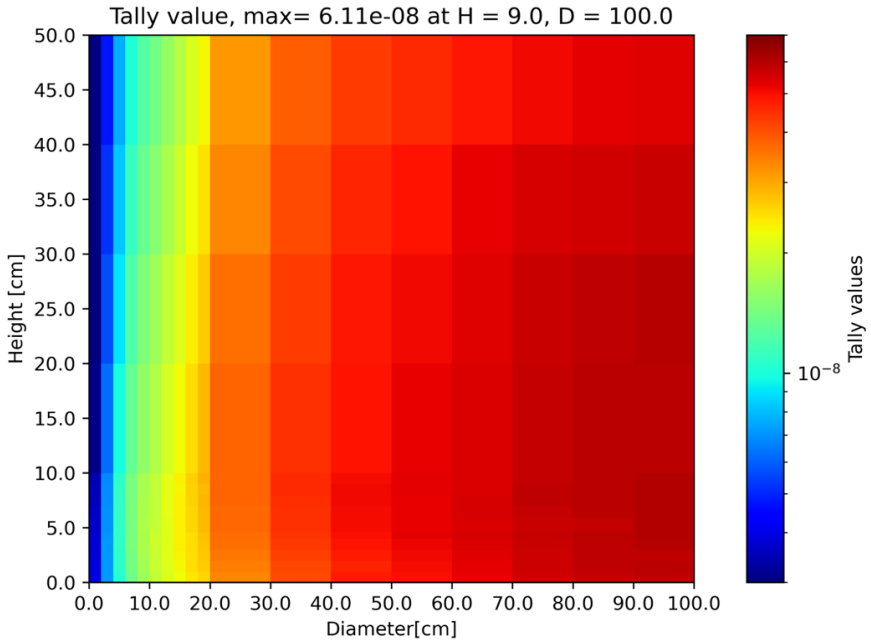

Figure 20-4 Neutron flux map for solid orthodeuterium, for neutrons between 20-40 [neutrons/source neutrons/ cm^2]

This project has received funding from the European Union's Horizon 2020 research and innovation programme under grant agreement No. 871072.

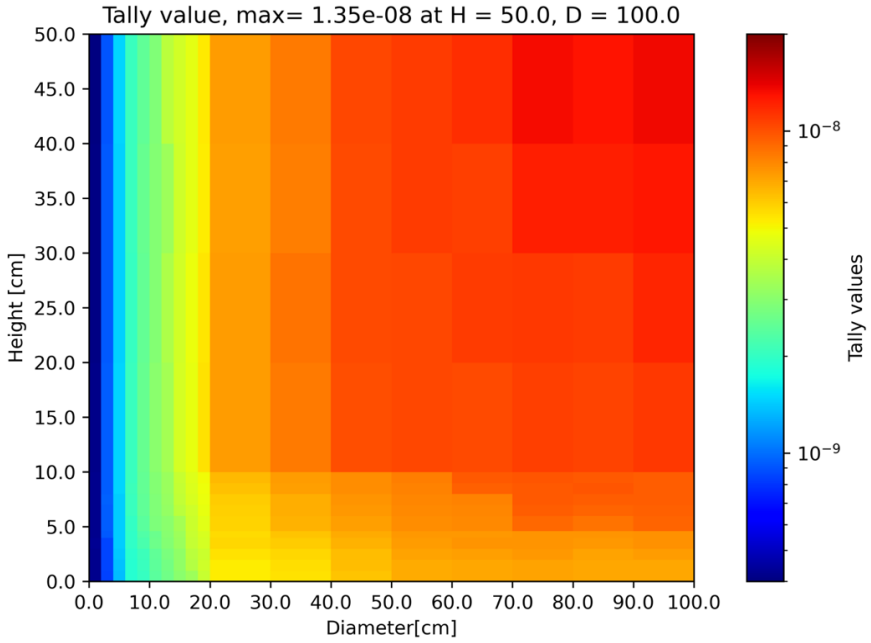

Figure 20-5 Neutron flux map for solid orthodeuterium, for neutrons above 40 Å [neutrons/source neutrons/ cm^2]

This project has received funding from the European Union's Horizon 2020 research and innovation programme under grant agreement No. 871072.

b. Solid paradeuterium at 5 K

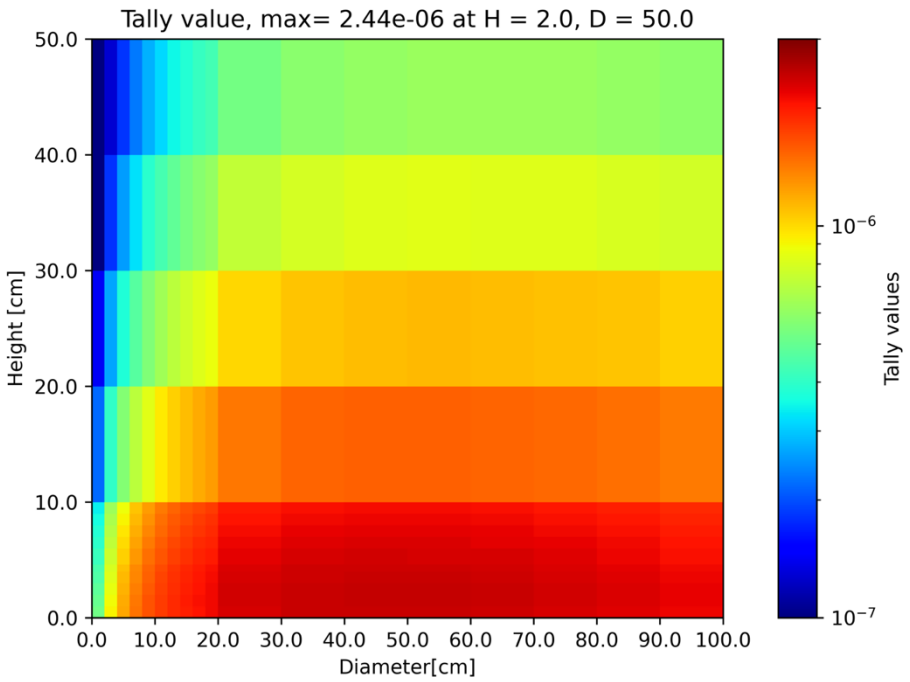

Figure 20-6 Neutron flux map for solid paradeuterium, neutrons between 2-4 Å [neutrons/source neutrons/ cm^2]

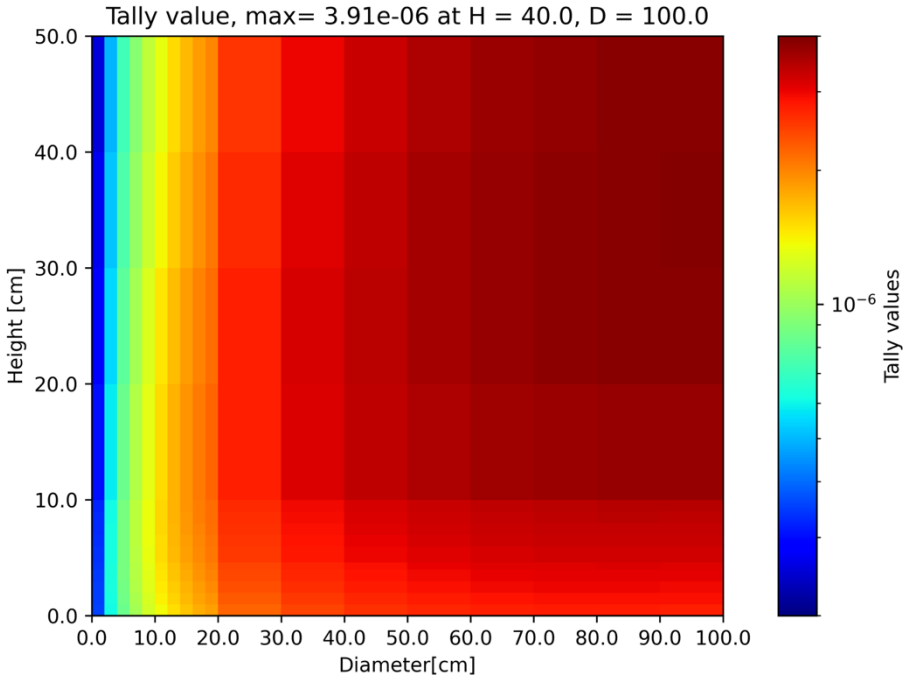

Figure 20-7 Neutron flux map for solid paradeuterium, neutrons between 4- 10 Å [neutrons/source neutrons/ cm^2]

This project has received funding from the European Union's Horizon 2020 research and innovation programme under grant agreement No. 871072.

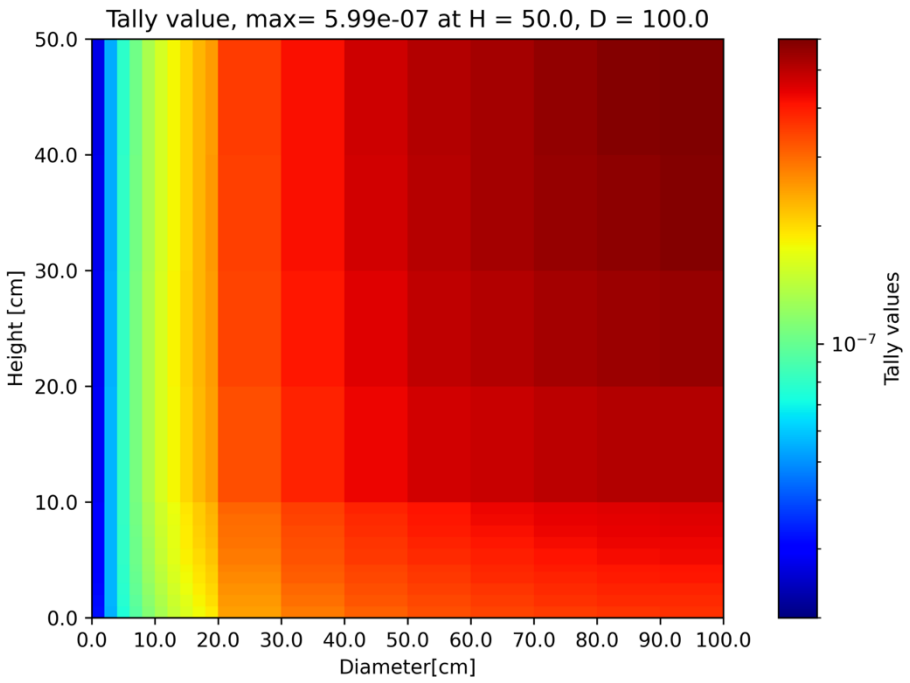

Figure 20-8 Neutron flux map for solid paradeuterium, neutrons between 10- 20 Å [neutrons/source neutrons/ cm^2]

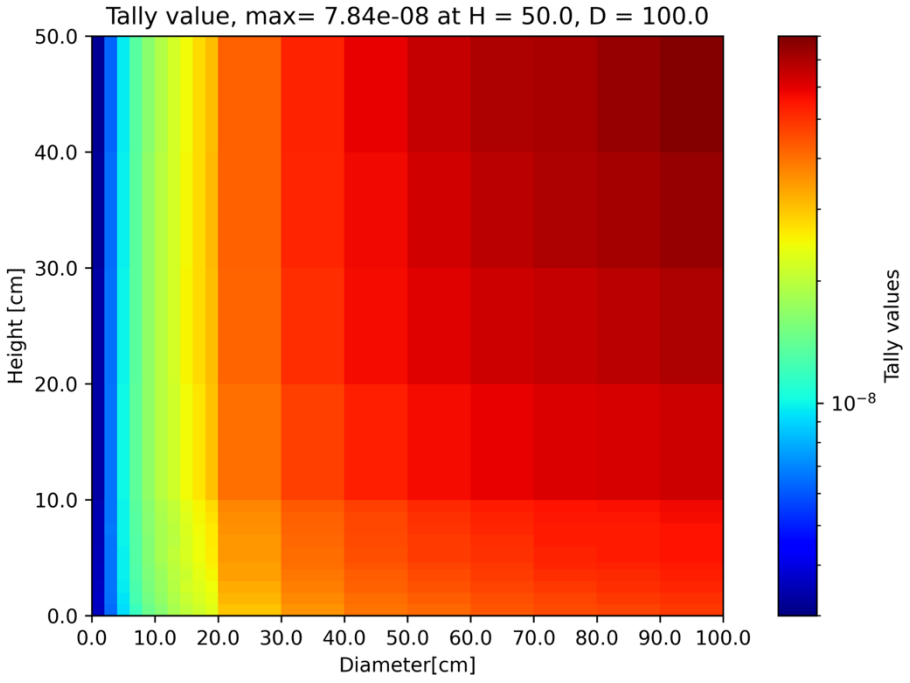

Figure 20-9 Neutron flux map for solid paradeuterium, neutrons between 20- 40 Å [neutrons/source neutrons/ cm^2]

This project has received funding from the European Union's Horizon 2020 research and innovation programme under grant agreement No. 871072.

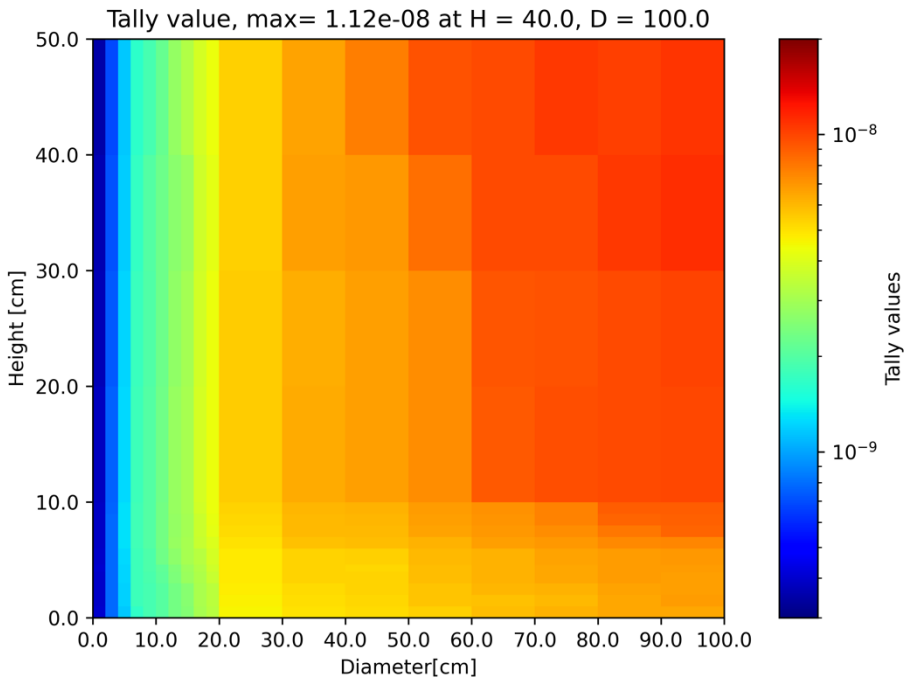

Figure 20-10 Neutron flux map for solid paradeuterium, neutrons above 40 Å [neutrons/source neutrons/ cm^2]

This project has received funding from the European Union's Horizon 2020 research and innovation programme under grant agreement No. 871072.

c. Liquid Orthohydrogen at 20 K

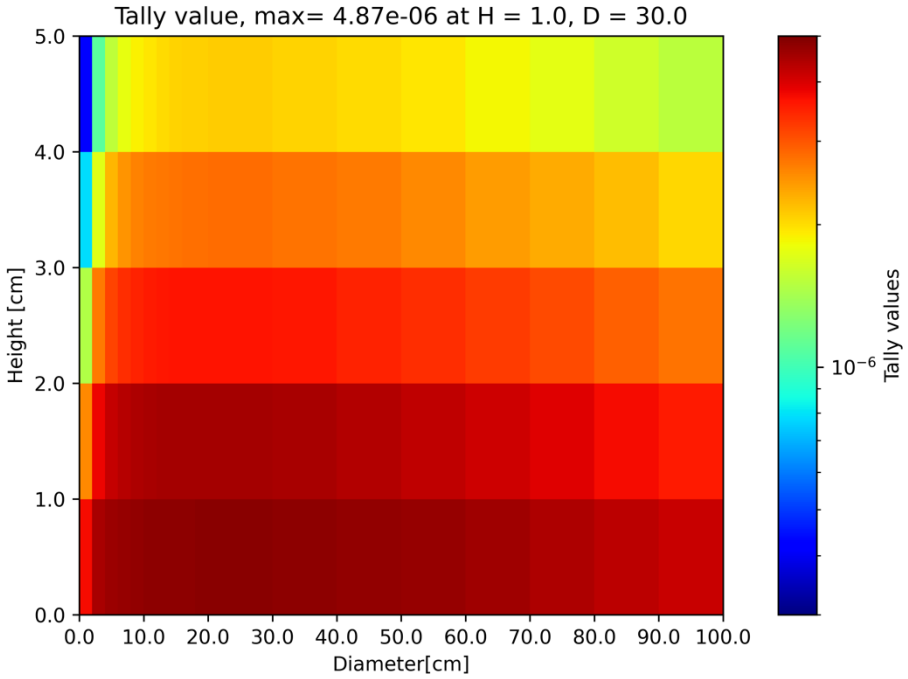

Figure 20-11 Neutron flux map for liquid orthohydrogen, neutrons between 2- 4 Å [neutrons/source neutrons/ cm^2]

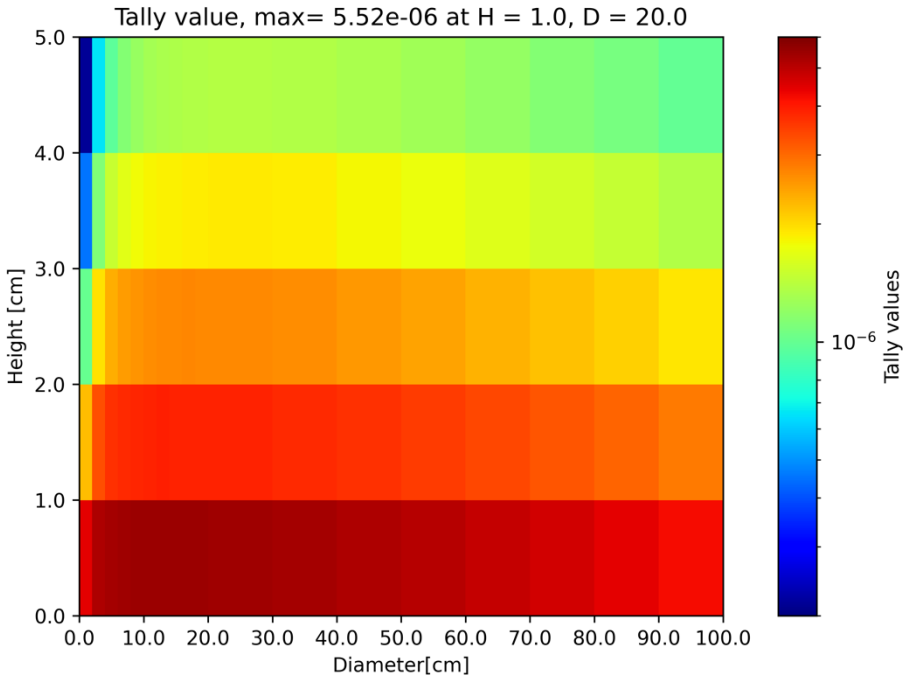

Figure 20-12 Neutron flux map for liquid orthohydrogen, neutrons between 4- 10 Å [neutrons/source neutrons/ cm^2]

This project has received funding from the European Union's Horizon 2020 research and innovation programme under grant agreement No. 871072.

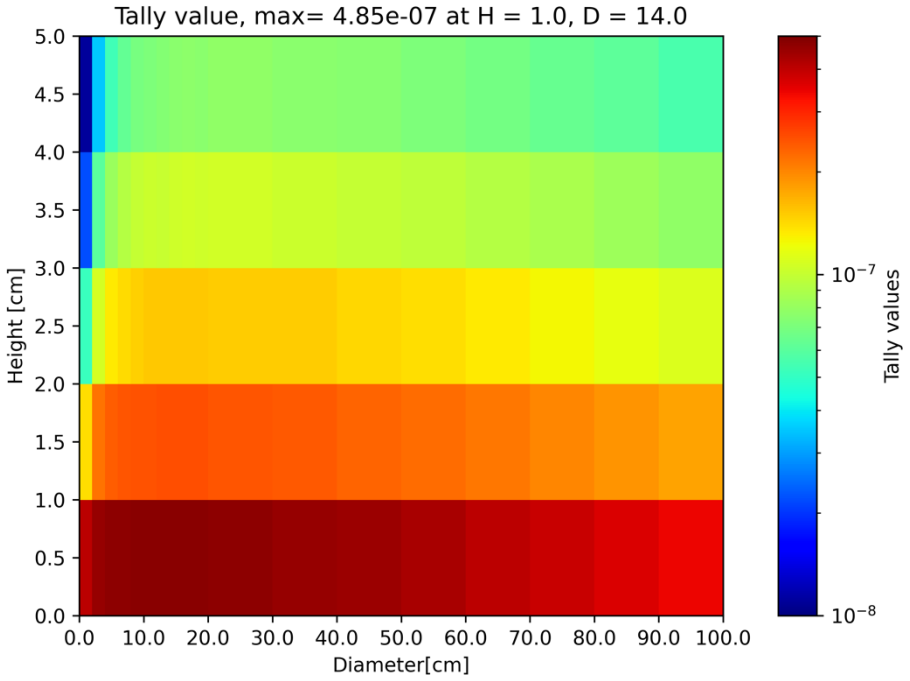

Figure 20-13 Neutron flux map for liquid orthohydrogen, neutrons between 10- 20 Å [neutrons/source neutrons/ cm^2]

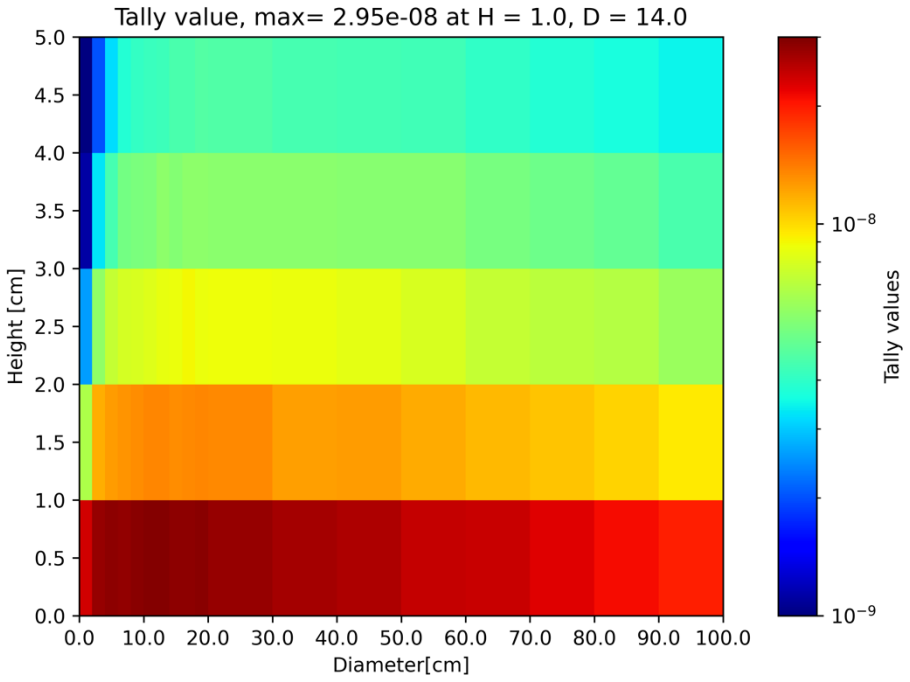

Figure 20-14 Neutron flux map for liquid orthohydrogen, neutrons between 20- 40 Å [neutrons/source neutrons/ cm^2]

This project has received funding from the European Union's Horizon 2020 research and innovation programme under grant agreement No. 871072.

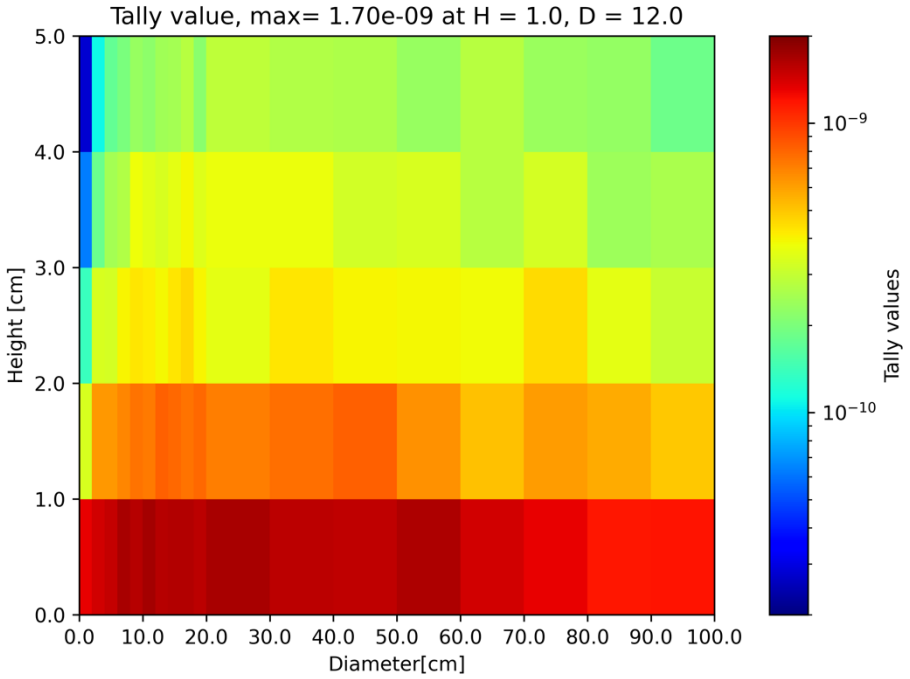

Figure 20-15 Neutron flux map for liquid orthohydrogen, neutrons. above 40 Å [neutrons/source neutrons/ cm^2]

This project has received funding from the European Union's Horizon 2020 research and innovation programme under grant agreement No. 871072.

d. Liquid Parahydrogen at 20 K

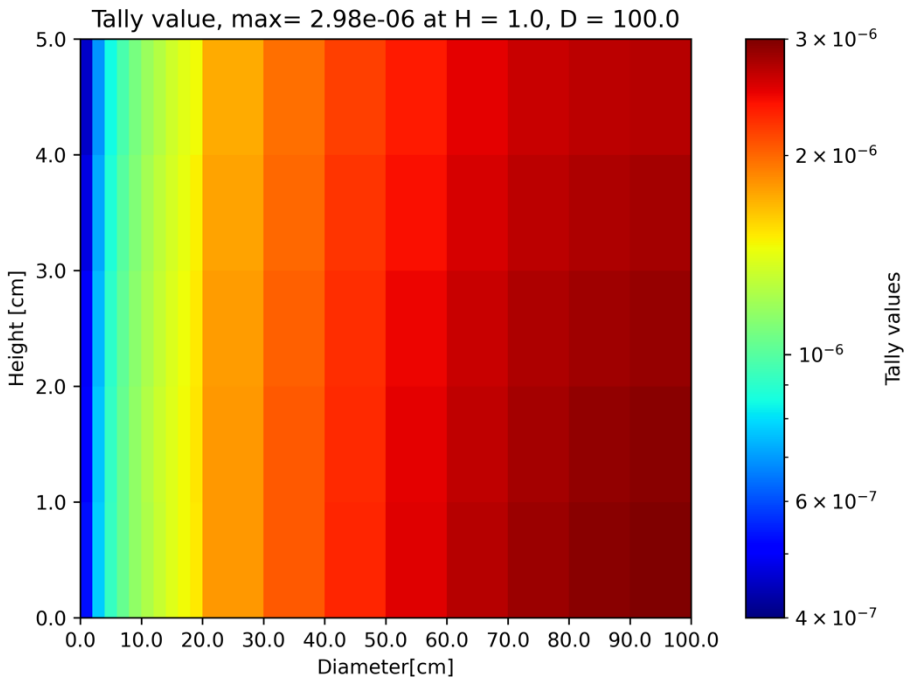

Figure 20-16 Neutron flux map for liquid parahydrogen, neutrons between 2- 4 Å [neutrons/source neutrons/ cm^2]

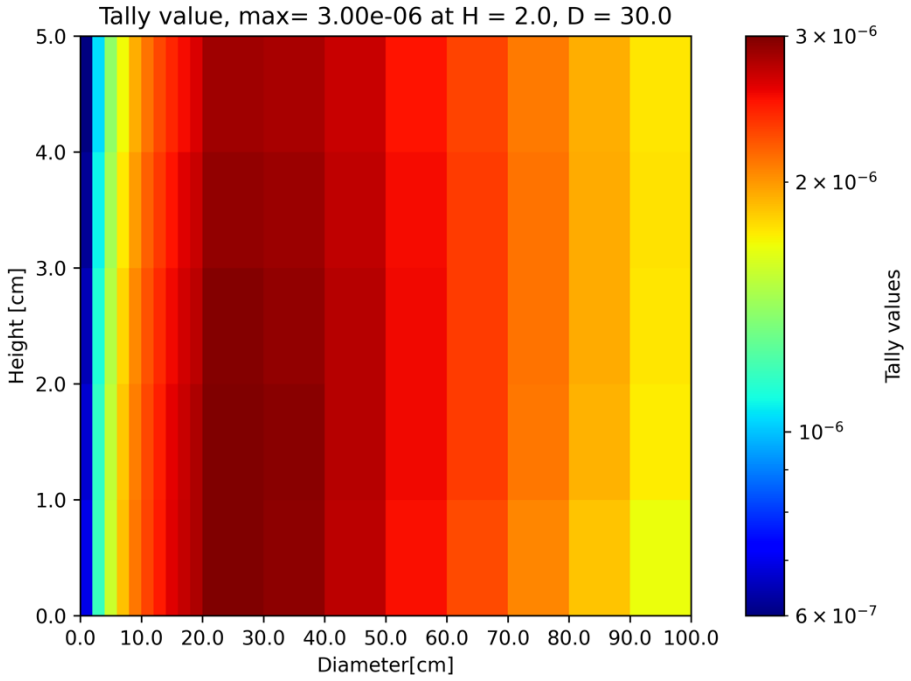

Figur 20-17 Neutron flux map for liquid parahydrogen, neutrons between 4-10 Å [neutrons/source neutrons/ cm^2]

This project has received funding from the European Union's Horizon 2020 research and innovation programme under grant agreement No. 871072.

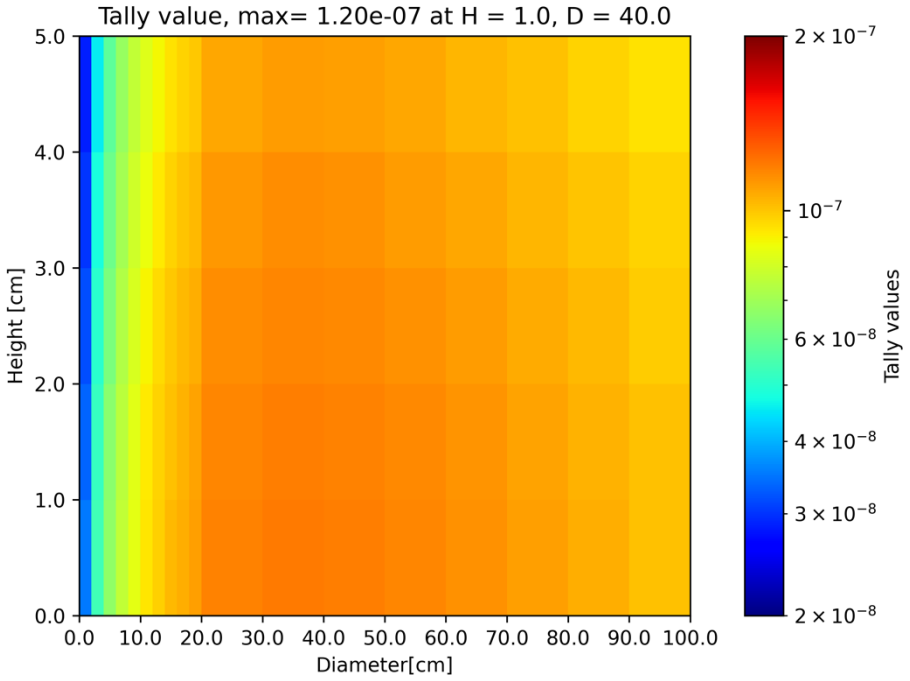

Figure 20-18 Neutron flux map for liquid parahydrogen, neutrons between 10-20 Å [neutrons/source neutrons/ cm^2]

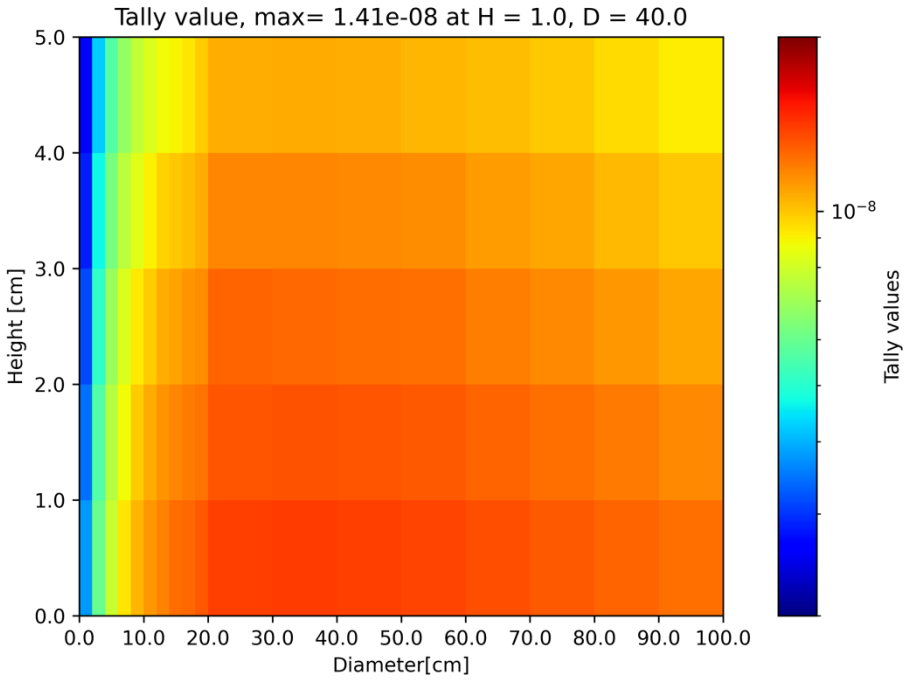

Figure 20-19 Neutron flux map for liquid parahydrogen, neutrons between 20-40 Å [neutrons/source neutrons/ cm^2]

This project has received funding from the European Union's Horizon 2020 research and innovation programme under grant agreement No. 871072.

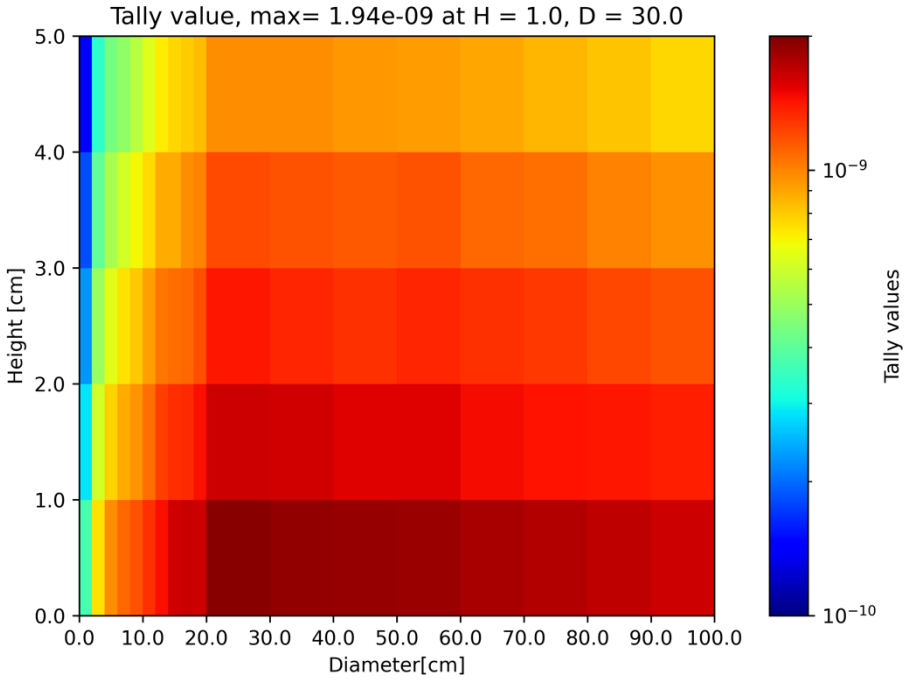

Figure 20-20 Neutron flux map for liquid parahydrogen, neutrons above 40 Å [neutrons/source neutrons/ cm^2]

This project has received funding from the European Union's Horizon 2020 research and innovation programme under grant agreement No. 871072.

e. Solid methane at 22 K

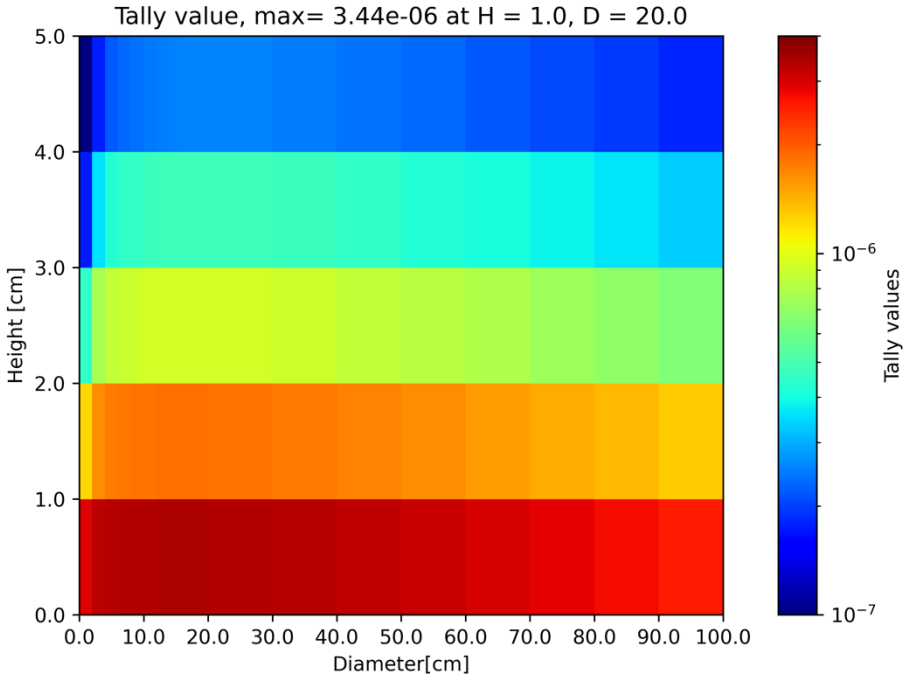

Figure 20-21 Neutron flux map for solid methane, neutrons between 2-4 Å [neutrons/source neutrons/ cm^2]

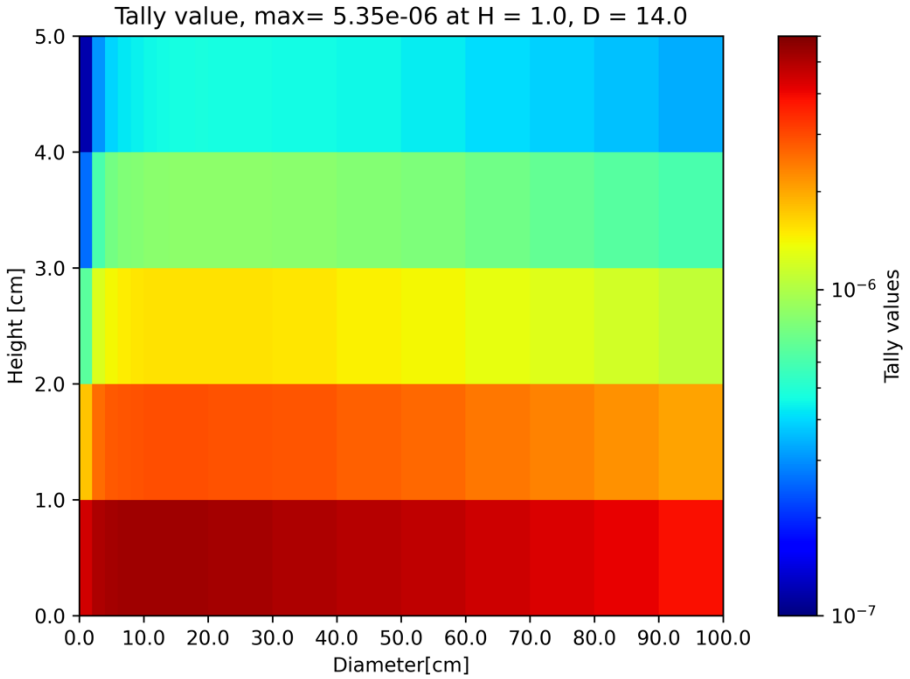

Figure 20-22 Neutron flux map for solid methane, neutrons between 4-10 Å [neutrons/source neutrons/ cm^2]

This project has received funding from the European Union's Horizon 2020 research and innovation programme under grant agreement No. 871072.

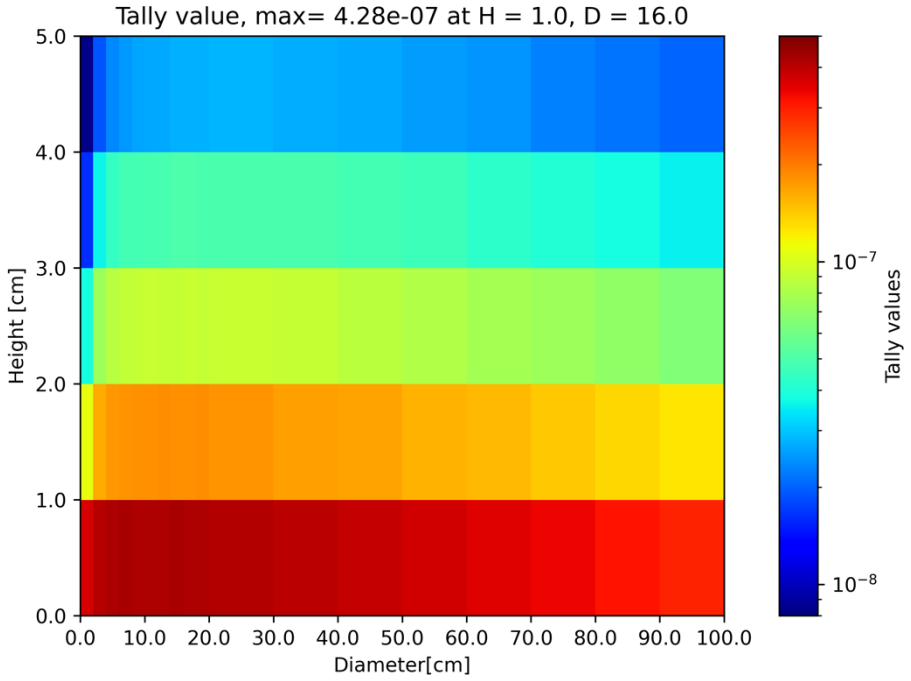

Figure 20-23 Neutron flux map for solid methane, neutrons between 10-20 Å [neutrons/source neutrons/ cm^2]

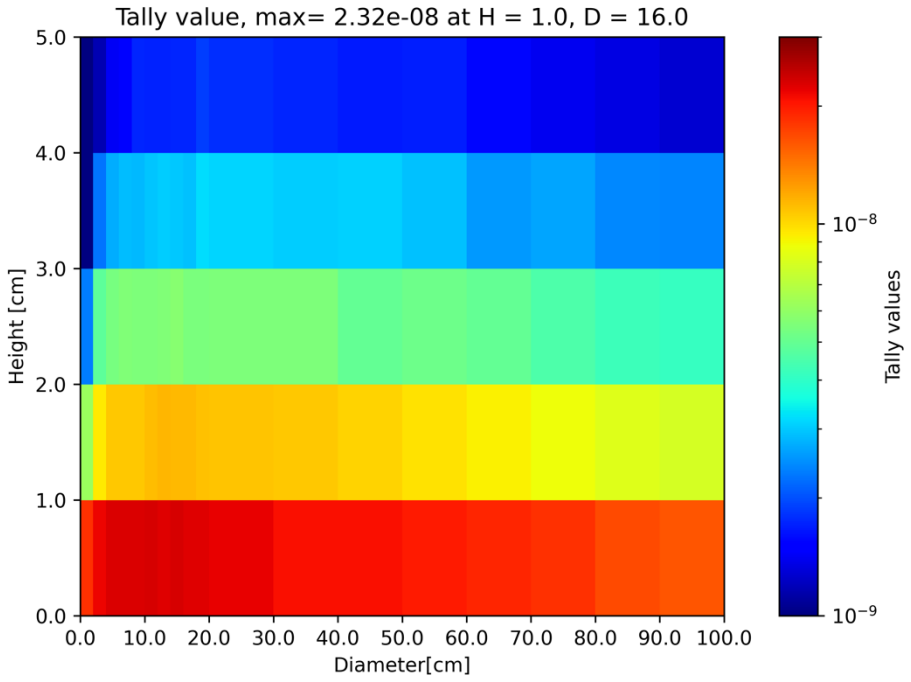

Figure 20-24 Neutron flux map for solid methane, neutrons between 20-40 Å [neutrons/source neutrons/ cm^2]

This project has received funding from the European Union's Horizon 2020 research and innovation programme under grant agreement No. 871072.

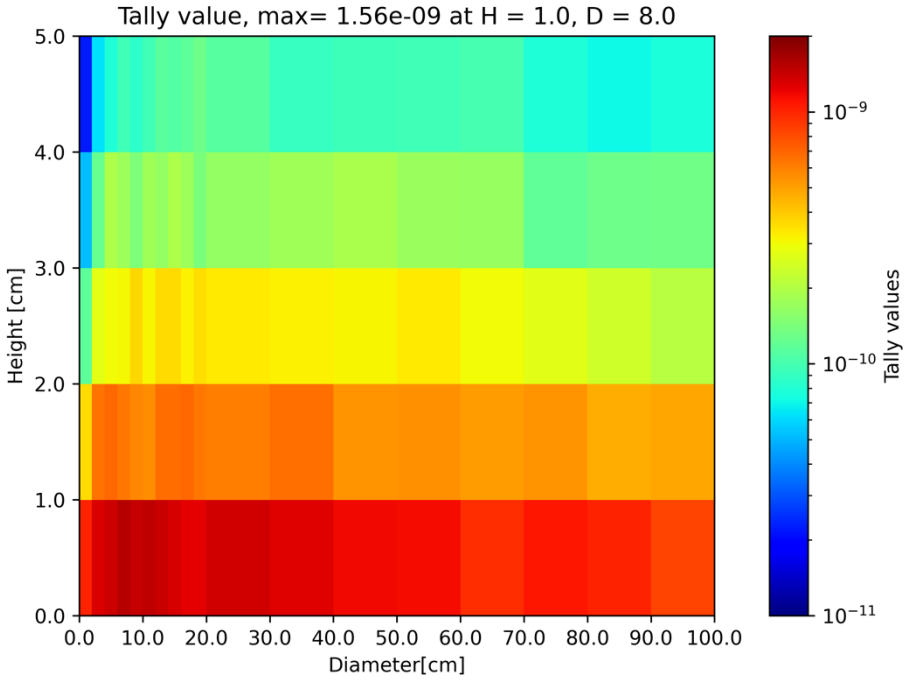

Figure 20-25 Neutron flux map for solid methane, neutrons above 40 Å [neutrons/source neutrons/ cm^2]

This project has received funding from the European Union's Horizon 2020 research and innovation programme under grant agreement No. 871072.

21 Bibliography

[1] C. Werner, MCNP Users Manual - Code Version 6.2, LA-UR-17-29981, 2017.

[2] *Connecting Russian and European Measures for Large-scale Research Infrastructures (CREMLINplus) proposal, Proposal number: 871072, HORIZON 2020,* 2020.

[3] K. Eder, M. Gruber and A. Zeilinger, "The new very cold neutron optics facility at ILL," *Nuclear Instruments and Methods A,* vol. 171, 1989.

[4] J. M. Carpenter and C. K. Loong, Elements of Slow-neutron Scattering, Cambridge University Press, 2015.

[5] B. J. Micklich and J. M. Carpenter, "Proceedings of the Workshop of a very cold neutron source," in *Intense Pulsed Neutron Source*, Argonne National Laboratory, 2005.

[6] B. Micklich, "Target Considerations for a Very Cold Neutron Source," in *Proceedings from the 3rd High-Power Targetry Workshop*, Bad Zurzach, Switzerland, 2007.

[7] V. V. Nesvizhevsky, "Reflectors for VCN and applications of VCN, February 2011," *Revista Mexicana de Fisica,* Vols. 57:1-5.

[8] V. V. Nesvizhevsky, *Nature Physics,* vol. 114, no. 6, 2010.

[9] M. Dewey, *Nuclear Instrum. Methods A.,* vol. 611, p. 189, 2009.

[10] F. Goennenwein, *Phys. Lett. B,* vol. 13, 2007.

[11] F. Mezei, L. Zanini, A. Takibayev, K. Batkov, E. Klinkby, E. Pitcher and T. Schönfeldt, "Low dimensional neutron moderators for enhanced source brightness," *Journal Neutron Research,* vol. 101, 2014.

[12] H. Abele, "Characterization of a ballistic supermirror neutron guide," *Nuclear Instruments and Methods in Physics Research Section A,* vol. 526, no. 1, pp. 407-417, 2006.

[13] V. V. Nesvizhevsky, Fluorinated nanodiamonds as unique neutron reflector, Journal of Neutron Research 20(4):1-3, December 2018.

[14] R. Cubitt, E. Lychagin, A. Muzychka, G. Nekhaev, V. Nesvizhevsky, G. Pignol, K. Protasov and A. Strelkov, "Quasi-specular reflection of cold neutrons from nano-dispersed media at above-critical angles," *Nuclear Instruments and Methods in Physics Research Section A,* vol. 622, no. 1, p. 182, 2010.

[15] V. V. Nesvizhevsky, E. Lychagin, A. Muzychka, A. Strelkov, G. Pignol and K. Protasov, "The reflection of very cold neutrons from diamond powder nanoparticles," *Nuclear Instruments and Methods in Physics Research Section A,* vol. 595, no. 3, p. 631, 2008.

[16] V. V. Nesvizhevsky, M. Dubois, P. Gutfreund, E. Lychagin, A. Nezvanov and K. Zhernenkov, "Effect of nano-diamond fluorination on the efficiency of quasispecular reflection of cold neutrons," *Physical Review A,* vol. 97, no. 2, p. 023629, 2018.

[17] M. Jamalipour, L. Zanini, E. Klinkby, G. Gorini and P. Willendrup, "Improved beam extraction at compact neutron sources using diamonds nanoparticles and supermirrors, 1033 (2022), 166719.," *Nucl. Instrum. Methods A,* vol. 1033, p. 166719., 2022.

[18] *ILL Yellow book.*

[19] A. Farkas, Ortho-Hydrogen, Para-Hydrogen, and Heavy Hydrogen, London: Cambridge University Press, 1935.

This project has received funding from the European Union's Horizon 2020 research and innovation programme under grant agreement No. 871072.

[20] I. A. Richardson and J. W. Leachman, "Fundamental Equation of State for Deuterium," *Journal of Physical and Chemical Reference Data ,* vol. 43, no. 013103, 2014.

[21] F. Gallmeier, T. Hugely, E. Iverson, W. Lu and I. Remec, "Options for a very cold neutron source for the second target station at SNS," *Journal of Physics Conference Series ,* vol. 1021, no. 1, p. 012083, 2018.

[22] V. Santoro, K. Andersen, M. Bernasconi, M. Bertelsen, Y. Beßler, D. Campi, V. Czamler and D. DiJulio, "Development of a High Intensity Neutron Source at the European Spallation Source: The HighNESS project," *arXiv:2204.04051,* 2022.

[23] O. Zimmer, "Neutron conversion and cascaded cooling in paramagnetic systems for a high-flux source of very cold neutrons," *Phys. Rev. C,* vol. 93, no. 3, p. 035503, 2016.

[24] J. Granada, J. I. Márquez Damián and C. Helman, "Studies on reflector materials for cold neutrons," *EPJ Web of Conferences,* vol. 231, p. 04002, 2020.

[25] P. Willendrup, E. Farhi, E. Knudsen, U. Filges, K. Lefmann and J. Stein, User and Programmers Guide to the Neutron Ray-Tracing Package McStas, version 3.1, Kongens Lyngby: Physics Department, Technical University of Denmark, 2021.

[26] F. X. Gallmeier, M. Wohlmuther, U. Filges, D. Kiselev and G. Muhrer, "Implementation of Neutron Mirror Modeling Capability into MCNPX and Its Demonstration in First Applications," *Nuclear Technology,* vol. 168, no. 3, pp. 768-772, 2009.

[27] Y. D. Harker and R. M. Brugger, "Investigation of the Low-Temperature Phase Transitions in Solid Methane by Slow Neutron Inelastic Scattering," *J. Chem. Phys.,* vol. 46, no. 2201, 1967.

[28] R. E. MacFarlane, D. W. Muir and R. M. Boicourt, "e NJOY Nuclear Data Processing System, Volume I: User's Manual," *LA-9393-M,* vol. 1, no. DE89, p. 011384, 1982.

[29] M. Teshigawara, "Measurement of neutron scattering cross section of nano-diamond with particle diameter of approximately 5 nm in energy range of 0.2 meV to 100 meV," *NIM A,* vol. 929, pp. 113-120, 2019.

[30] K. Ramić, J. I. Marquez Damian, T. Kittelmann and D. DiJulio, "NJOY+ NCrystal: An open-source tool for creating thermal neutron scattering libraries with mixed elastic support," *Nuclear Instruments and Methods in Physics Research Section A,* vol. 1027, no. 166227, 2022.

[31] J. R. Granada, "Neutron scattering kernel for solid deuterium," *Europhysics Letters,* vol. 86, no. 66007, 2009.

[32] A. J. M. Plompen, O. Cabellos, C. De Saint Jean, M. Fleming, A. Algora, M. Angelone and P. Archier, "The joint evaluated fission and fusion nuclear data library, JEFF-3.3," *The European Physical Journal,* vol. A 56, no. 1-108, 2020.

[33] J. Granada, V. H. Gillette, M. E. Pepe and M. M. Sbaffoni, "Improved thermal neutron scattering kernels for liquid hydrogen and deuterium," *Journal of Neutron Research,* vol. 11, no. 25-40, 2003.

[34] J. M. Damian, D. DiJulio and G. Muhrer, "Nuclear data development at the European Spallation Source," *Journal of Neutron Research Preprint,* vol. 23, no. 157, 2021.

[35] C. Werner, User's Manual Code Version 6.2, LA-UR-17-29981, 2017.

[36] L. Zanini, E.Klinkby, F. Mezei and A. Takibayev, "Low-dimensional moderators at ESS and compact neutron sources," *The European Physical Journal Conferences,* vol. 231, no. 04006, 2020.

This project has received funding from the European Union's Horizon 2020 research and innovation programme under grant agreement No. 871072.

This project has received funding from the European Union's Horizon 2020 research and innovation programme under grant agreement No. 871072.